

Quantitation of the pD Dependent Thermodynamics of the N \rightleftharpoons S Pseudorotational Equilibrium of the Pentofuranose Moiety in Nucleosides Gives a Direct Measurement of the Strength of the Tunable Anomeric Effect and the pK_a of the Nucleobase[†]

C. Thibaudeau, J. Plavec, and J. Chattopadhyaya*

Department of Bioorganic Chemistry, Box 581, Biomedical Centre, University of Uppsala, S-751 23 Uppsala, Sweden

Received June 21, 1995[®]

The anomeric and the gauche effects are two competing stereoelectronic forces that drive the North (N) (C2'-*exo*-C3'-*endo*) \rightleftharpoons South (S) (C2'-*endo*-C3'-*exo*) pseudorotational equilibrium in nucleosides. The quantitation of the energetics of pD dependent N \rightleftharpoons S pseudorotational equilibria of the pentofuranose moiety in 2'-deoxyribonucleosides **1–6**, 1'-imidazolyl-2'-deoxy- β -D-ribofuranose **7**, and ribonucleosides **8–13** shows that the strength of the anomeric effect of the constituent heterocyclic moiety at C1' is dependent upon the unique aromatic nature of the nucleobase, which is tuned by the pD of the medium. The force that drives the protonation \rightleftharpoons deprotonation equilibrium of the heterocyclic nucleobases in nucleosides is transmitted through the anomeric effect to drive the two-state N \rightleftharpoons S pseudorotational equilibrium of the constituent furanose: (i) The enhanced strength ($\Delta\Delta H^{\circ}_{(P-N)}$) of the anomeric effect in the protonated (P) nucleoside compared to the neutral (N) form is experimentally evidenced by the increased preference of sugar for N-type conformation and of the nucleobase in the pseudoaxial orientation in the former by $\Delta\Delta H^{\circ}_{(P-N)}$ of 3.2 kJ/mol for dA (**1**), 4.9 kJ/mol for dG (**2**), 0.7 kJ/mol for dC (**3**), 2.3 kJ/mol for dImb (**7**), 4.2 kJ/mol for A (**8**), 8.7 kJ/mol for G (**9**), and 2.9 kJ/mol for C (**10**). (ii) In contrast, the S-type sugar conformer, which places the nucleobase in pseudoequatorial orientation, is considerably more preferred in the alkaline medium owing to the weakening of the anomeric effect in the N1-deprotonated D-guanine and N3-deprotonated uracil, 5-fluorouracil, or thymine moieties compared to the neutral counterparts by $\Delta\Delta H^{\circ}_{(N-D)}$ of 2.1 kJ/mol for dG (**2**), 0.7 kJ/mol for dU (**4**), 0.5 kJ/mol for T (**5**), 0.3 kJ/mol for FdU (**6**), 4.3 kJ/mol for G (**9**), 1.7 kJ/mol for U (**11**), 1.5 kJ/mol for rT (**12**), and 1.5 kJ/mol for FU (**13**). This has allowed us to independently measure the pK_a of constituent heterocyclic nucleobases by the quantitation of the pD dependent energetics of the two-state N \rightleftharpoons S pseudorotational equilibrium.

Introduction

The primary structure of a nucleoside is made of a purine or a pyrimidine aglycon (adenine, guanine, cytosine, uracil, thymine, and several other modified heterocycles) which is covalently bonded from N9 of purine or N3 of pyrimidine to C1' of a D-ribo or D-2'-deoxyribo-pentofuranose in a β -configuration. While the aglycon moieties of the nucleoside are directly involved in carrying the genetic information and its propagation in the replication machinery by Watson–Crick or Hoogsteen

hydrogen bonded base-pairing, very little is, however, known about how the aglycon and the constituent pentofuranose moiety form the steric and stereoelectronic partnership that make the nucleic acids perform unique roles such as the storehouse of genetic information (DNA) and in their selective expression, in the processing of pre-mRNA through lariat-RNA intermediates (Splicing), in the propagation of tumor viruses, in the catalysis, in the cellular differentiation and in the development in cancer induction.

The sugar moieties of nucleosides are puckered and in solution are involved in a two-state N \rightleftharpoons S pseudorotational equilibrium (Scheme 1) which is energetically controlled¹ by various competing stereoelectronic effects (*i.e.*, anomeric^{2a-d,3-8} and gauche^{2e-j} effects). There are other important factors which also determine the pre-

[†] Dedicated to Prof. C. B. Reese on the occasion of his 65th birthday.

[®] Abstract published in *Advance ACS Abstracts*, December 15, 1995.

(1) (a) Plavec, J.; Tong, W.; Chattopadhyaya, J. *J. Am. Chem. Soc.* **1993**, *115*, 9734. (b) Plavec, J.; Garg, N.; Chattopadhyaya, J. *J. Chem. Soc., Chem. Commun.* **1993**, 1011. (c) Plavec, J.; Koole, L. H.; Chattopadhyaya, J. *J. Biochem. Biophys. Meth.* **1992**, *25*, 253. (d) Koole, L. H.; Buck, H. M.; Nyilas, A.; Chattopadhyaya, J. *Can J. Chem.* **1987**, *65*, 2089. (e) Koole, L. H.; Buck, H. M.; Bazin, H.; Chattopadhyaya, J. *Tetrahedron* **1987**, *43*, 2289. (f) Koole, L. H.; Plavec, J.; Liu, H.; Vincent, B. R.; Dyson, M. R.; Coe, P. L.; Walker, R. T.; Hardy, G. W.; Rahim, S. G.; Chattopadhyaya, J. *J. Am. Chem. Soc.* **1992**, *114*, 9934. (g) Plavec, J.; Thibaudeau, C.; Viswanadham, G.; Sund, C.; Chattopadhyaya, J. *J. Chem. Soc., Chem. Comm.* **1994**, 781. (h) Thibaudeau, C.; Plavec, J.; Watanabe, K. A.; Chattopadhyaya, J. *J. Chem. Soc., Chem. Commun.* **1994**, 537. (i) Thibaudeau, C.; Plavec, J.; Garg, N.; Panchikhin, A.; Chattopadhyaya, J. *J. Am. Chem. Soc.* **1994**, *116*, 4038. (j) Plavec, J.; Thibaudeau, C.; Chattopadhyaya, J. *J. Am. Chem. Soc.* **1994**, *116*, 6558. (k) Thibaudeau, C.; Plavec, J.; Chattopadhyaya, J. *J. Am. Chem. Soc.* **1994**, *116*, 8033. (l) Plavec, J.; Thibaudeau, C.; Chattopadhyaya, J. *Tetrahedron* **1995**, *51*, 11775. (m) For the latest regression analysis of the experimental thermodynamics of N \rightleftharpoons S pseudorotational equilibrium on 18 different nucleosides and abasic sugars giving the relative strengths of anomeric and gauche effects associated with each compound, see: Plavec, J. Ph.D. Thesis, Department of Bioorganic Chemistry, Uppsala University, Sweden, **1995** (Fax: +4618-55 44 95).

(2) (a) Tvaroska, I.; Bleha, T. *Adv. Carbohydr. Chem.* **1989**, *47*, 45. (b) Juaristi, E.; Cuevas, G. *Tetrahedron* **1992**, *48*, 5019. (c) Petillo, P. A.; Lerner, L. A. In *The Anomeric Effect and Associated Stereoelectronic Effects*; Thatcher, G. R. J., Ed.; ACS Symposium Series; American Chemical Society: Washington, DC, **1993**; p 156. (d) Box, V. G. S. *Heterocycles* **1990**, *31*, 1157. (e) Olson, W. K.; Sussman, J. L. *J. Am. Chem. Soc.* **1982**, *104*, 270. (f) Olson, W. K. *J. Am. Chem. Soc.* **1982**, *104*, 278. (g) Phillips, L.; Wray, V. J. *J. Chem. Soc., Chem. Commun.* **1973**, 90. (h) Brunck, T. K.; Weinhold, F. *J. Am. Chem. Soc.* **1979**, *101*, 1700. (i) Murcko, M. A.; DiPaola, R. A. *J. Am. Chem. Soc.* **1992**, *114*, 10010. (j) Wiberg, K. B.; Murcko, M. A.; Laidig, K. E.; MacDougall, P. J. *J. Phys. Chem.* **1990**, *94*, 6956.

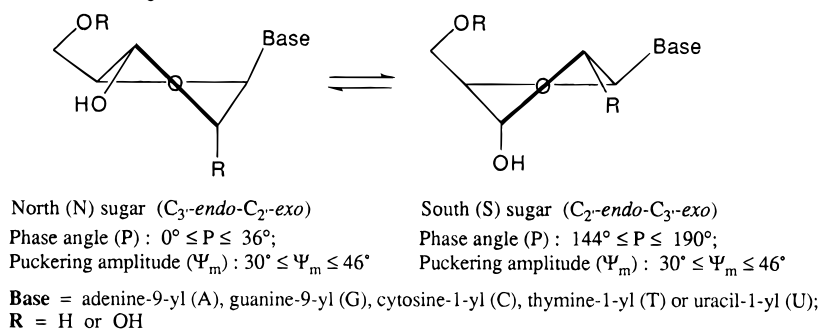
(3) Edward, J. T. *Chem. Ind. (London)* **1955**, 1102.

(4) (a) Lucken, E. A. C. *J. Chem. Soc.* **1959**, 2954. (b) Romers, C.; Altona, C.; Buys, H. R.; Havinga, E. *Top. Stereochem.* **1969**, *4*, 39.

(5) Saenger, W. *Principles of Nucleic Acid Structure*; Springer Verlag: Berlin, **1988**.

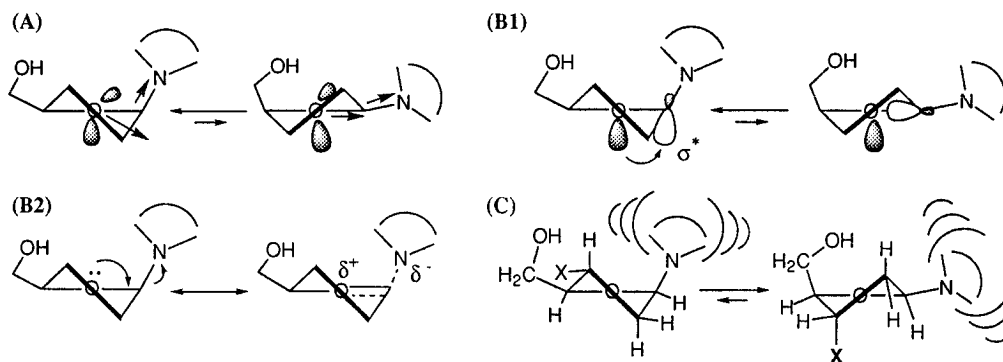
(6) Perrin, C. L.; Armstrong, K. B.; Fabian, M. A. *J. Am. Chem. Soc.* **1994**, *116*, 715.

Scheme 1. Dynamic Two-State Pseudorotational Equilibrium of the β -D-Pentofuranose Moiety Determined by the Nature and Relative Orientations of Substituents^a



^a The involvement of 2'-OH in the gauche effects with O4', O3' and anomeric N atom as well as other intramolecular interactions are responsible for the conformational differences¹ between DNA and RNA.

Scheme 2. Dynamic Two-State N \rightleftharpoons S Pseudorotational Equilibrium (See Scheme 1) Driven by the Anomeric Effect of the Heterocyclic Moiety (A, C, G, U, or T) at C1' with β Configuration^a



^a The resulting stabilizing influence due to the anomeric effect (see ref 5, p 70 for the geometrical implication of anomeric effect) can be attributed either to electrostatic repulsion (A) or hyperconjugative $n(O) \rightarrow \sigma^*_{C1'-N}$ molecular orbital delocalization (B1/B2). The inherent steric effect of the nucleobase shown in panel C opposes the stabilization of N conformers due to the stereoelectronic contribution of the anomeric effect (see ref 1).

ferred state of N \rightleftharpoons S pseudorotational equilibrium such as base-base stacking, hydration, steric effects, or inter- and intramolecular H-bonding or by the conformational constraints imposed by the ring closure as in the lariat-RNA.

We have shown earlier by the detailed comparative analysis of temperature-dependent conformational preferences of the two-state N \rightleftharpoons S sugar equilibrium in a series of 1-deoxy-, 1,2-dideoxy-, and 1,2,3-trideoxypentofuranoses with those of the furanose moieties in adenosine, guanosine, thymidine, uridine, and cytidine and their 2'-deoxy and 2',3'-dideoxy counterparts that the strength of the anomeric effect in nucleosides increases in the following order: adenine [$\Delta H^{\circ} = 2.1 \pm 1.0$ kJ/mol] < guanine [$\Delta H^{\circ} = 3.1 \pm 1.0$ kJ/mol] < thymine [$\Delta H^{\circ} = 3.7 \pm 0.9$ kJ/mol] < uracil [$\Delta H^{\circ} = 4.5 \pm 0.9$ kJ/mol] < cytosine [$\Delta H^{\circ} = 5.2 \pm 0.9$ kJ/mol].^{1a,m} We have also shown that the drive of the N \rightleftharpoons S pseudorotational equilibria by the anomeric effect can be tuned by the inherent gauche effects of [O3'-C3'-C4'-O4'], [O2'-C2'-C1'-O4'], and [O2'-C2'-C1'-N] fragments.¹ The fluctuations of the experimentally observed nucleobase-dependent strengths of the anomeric effects (Scheme 2) within the ribo-, 2'-deoxyribo-, or 2,3'-dideoxyribonucleosides reflect two competing inherent properties of nucleosides: (i) different abilities of their glycosidic bonds to adopt antiperiplanar orientations with respect to the

constituent O4' lone pair either through electrostatic repulsions^{2a-d,6} or $n \rightarrow \sigma^*$ molecular orbital interaction,^{2a-d,4,7,8} which drives the N \rightleftharpoons S sugar equilibrium to N-type conformation, and (ii) the specific steric effect that is associated with each of the heterocyclic bases and the extent of the steric pressure that it exerts on the drive of the N \rightleftharpoons S pseudorotational equilibrium toward the sterically preferred S-type conformers. Thus, the strength of the anomeric effect in a nucleoside can be assessed in a quantitative manner by monitoring the preference of its sugar moiety for N-type (*i.e.*, pseudoaxial aglycon) versus S-type (*i.e.*, pseudoequatorial aglycon) conformations. This has led us in a recent work^{1k} to dissect the steric and stereoelectronic components of the anomeric effect of adenine and guanine bases in adenosine and guanosine through the comparison of the pseudorotational equilibria of these N-ribonucleosides with those of the C-nucleosides, formycin A and formycin B.

Since each neutral heterocyclic base¹ in a nucleoside has the characteristic anomeric effect it was clear to us that the change of the electronic character of purine and pyrimidine bases in nucleosides **1-13** (Chart 1) either by protonation or by deprotonation should result in the modulation of the strength of the anomeric effect, which should be observable by monitoring the changes in the bias of the N \rightleftharpoons S pseudorotational equilibria. A study of the magnitudes of the downfield shifts of ¹⁵N-NMR resonances ($\Delta\delta$) of the glycosyl-nitrogens in purine and pyrimidine nucleosides upon addition of 1 equiv of trifluoroacetic acid in the DMSO solution is also consis-

(7) Salzner, U. *J. Org. Chem.* **1995**, *60*, 986.

(8) Cosse-Barbi, A.; Watson, D. G.; Dubois, J. E. *Tetrahedron Lett.* **1989**, *30*, 163.

Table 1. pH-Dependent Thermodynamics of the Two-State N \rightleftharpoons S Equilibrium in dA (1) and A (8)

dA (1)						A (8)					
pD ^a	ΔH° (°) ^{b,c}	ΔS° (°) ^{c,d}	$-T\Delta S^{\circ}$ ^b	ΔG° ^b	%S ²⁹⁸ ^e	pD ^a	ΔH° (°) ^{b,c}	ΔS° (°) ^{c,d}	$-T\Delta S^{\circ}$ ^b	ΔG° ^b	%S ²⁹⁸ ^e
1.5	-1.1 (0.1)	0.1 (0.1)	0.0	-1.1	61	1.2	-0.5 (0.1)	0.0 (0.3)	0.0	-0.5	55
2.1	-0.9 (0.1)	0.8 (0.1)	-0.2	-1.1	61	1.9	-0.4 (0.1)	0.8 (0.3)	-0.2	-0.6	56
2.6	-0.8 (0.1)	1.2 (0.1)	-0.4	-1.2	62	2.4	-0.2 (0.1)	1.4 (0.4)	-0.4	-0.6	56
3.0	-0.8 (0.1)	1.8 (0.1)	-0.5	-1.3	63	2.9	-0.4 (0.1)	1.2 (0.3)	-0.4	-0.8	58
3.4	-1.4 (0.1)	0.3 (0.1)	-0.1	-1.5	65	3.4	-1.7 (0.2)	-2.3 (0.4)	0.7	-1.0	60
3.6	-2.1 (0.1)	-1.6 (0.2)	0.5	-1.6	66	3.7	-2.6 (0.2)	-4.6 (0.4)	1.4	-1.2	62
3.8	-2.3 (0.1)	-1.8 (0.2)	0.5	-1.8	67	4.3	-4.2 (0.3)	-8.4 (0.4)	2.5	-1.7	66
4.1	-3.2 (0.2)	-4.4 (0.3)	1.3	-1.9	68	5.0	-4.2 (0.3)	-8.2 (0.5)	2.4	-1.8	67
4.5	-3.4 (0.1)	-4.9 (0.7)	1.5	-1.9	69	5.7	-4.2 (0.3)	-8.3 (0.5)	2.5	-1.7	67
5.0	-3.6 (0.2)	-5.3 (0.7)	1.6	-2.0	69	6.5	-4.1 (0.3)	-7.8 (0.5)	2.3	-1.8	67
6.1	-3.8 (0.2)	-5.9 (0.7)	1.8	-2.0	69						

^a Our pD values are given by a pH meter equipped with a calomel electrode calibrated with standard buffers at pH 4 and 7 in H₂O and are not corrected for the deuterium isotope effect. ^b At 298 K, in kJ/mol. ^c ΔH° and ΔS° values are average values and have been calculated using the procedure described in the Experimental Section. ^d In J/molK. ^e %S²⁹⁸ values were calculated from the corresponding ΔG° using the relation: %S²⁹⁸ = 100[exp(- $\Delta G^{\circ}/RT$)]/[exp(- $\Delta G^{\circ}/RT$) + 1].

Table 2. pH-Dependent Thermodynamics of the Two-State N \rightleftharpoons S Equilibrium in dG (2) and G (9)

dG (2)						G (9)					
pD ^a	ΔH° (°) ^{b,c}	ΔS° (°) ^{c,d}	$-T\Delta S^{\circ}$ ^b	ΔG° ^b	%S ²⁹⁸ ^e	pD ^a	ΔH° (°) ^{b,c}	ΔS° (°) ^{c,d}	$-T\Delta S^{\circ}$ ^b	ΔG° ^b	%S ²⁹⁸ ^e
1.0	1.8 (0.1)	6.7 (0.2)	-2.0	-0.2	52	0.6	4.9 (0.2)	11.8 (0.8)	-3.5	1.4	36
1.2	1.5 (0.1)	5.6 (0.2)	-1.7	-0.2	52	0.9	4.6 (0.2)	11.0 (0.8)	-3.3	1.3	37
1.5	1.5 (0.1)	5.7 (0.1)	-1.7	-0.2	52	1.2	4.6 (0.2)	11.6 (0.4)	-3.4	1.1	39
1.8	1.7 (0.1)	7.0 (0.2)	-2.1	-0.4	54	1.5	5.1 (0.2)	14.0 (0.3)	-4.2	0.9	41
2.2	1.7 (0.1)	8.8 (0.2)	-2.6	-0.9	59	1.8	5.1 (0.1)	15.5 (0.2)	-4.6	0.5	45
2.5	0.5 (0.1)	5.8 (0.1)	-1.7	-1.2	62	1.9	4.8 (0.1)	15.2 (0.2)	-4.5	0.3	47
2.8	-0.9 (0.1)	1.9 (0.1)	-0.6	-1.5	64	2.3	2.8 (0.1)	10.5 (0.2)	-3.1	-0.3	53
3.0	-1.8 (0.1)	-0.7 (0.7)	0.2	-1.6	65	2.7	-0.5 (0.1)	1.8 (0.3)	-0.5	-1.0	60
3.2	-2.0 (0.1)	-1.4 (0.7)	0.4	-1.6	65	3.0	-2.3 (0.2)	-3.6 (0.5)	1.1	-1.2	62
3.6	-2.6 (0.1)	-3.0 (0.7)	0.9	-1.7	66	3.6	-3.3 (0.2)	-6.1 (0.6)	1.8	-1.5	65
4.0	-2.5 (0.1)	-2.7 (0.7)	0.8	-1.7	66	4.4	-3.3 (0.2)	-6.0 (0.7)	1.8	-1.5	65
5.0	-2.8 (0.1)	-3.8 (0.7)	1.1	-1.7	66	6.4	-3.3 (0.2)	-5.9 (0.7)	1.8	-1.5	65
6.2	-2.4 (0.1)	-2.4 (0.7)	0.7	-1.7	66	7.5	-3.4 (0.2)	-6.3 (0.7)	1.9	-1.5	65
7.5	-2.8 (0.1)	-3.4 (0.7)	1.0	-1.8	67	8.5	-4.0 (0.2)	-7.8 (0.7)	2.3	-1.7	66
8.4	-3.2 (0.1)	-4.5 (0.7)	1.3	-1.9	68	9.1	-4.6 (0.3)	-9.0 (0.6)	2.7	-1.9	68
8.9	-3.4 (0.1)	-4.8 (0.7)	1.4	-2.0	69	9.4	-4.9 (0.3)	-9.4 (0.6)	2.8	-2.1	70
9.3	-3.9 (0.1)	-5.9 (0.7)	1.8	-2.1	70	9.7	-5.8 (0.4)	-11.6 (0.5)	3.5	-2.3	72
9.7	-4.1 (0.1)	-5.7 (0.6)	1.7	-2.4	72	10.0	-6.0 (0.4)	-12.0 (0.6)	3.6	-2.4	73
10.0	-4.3 (0.1)	-6.1 (0.6)	1.8	-2.5	73	10.4	-6.7 (0.5)	-13.8 (0.7)	4.1	-2.6	74
10.5	-4.5 (0.2)	-6.3 (0.6)	1.9	-2.6	74	10.9	-7.6 (0.6)	-16.1 (0.7)	4.8	-2.8	76
10.9	-5.0 (0.2)	-7.5 (0.6)	2.2	-2.8	75	11.5	-7.5 (0.5)	-15.7 (0.7)	4.7	-2.8	76
11.4	-5.0 (0.2)	-7.7 (0.6)	2.3	-2.7	75	12.0	-7.8 (0.6)	-16.6 (0.8)	4.9	-2.9	76

^a Our pD values are given by a pH meter equipped with a calomel electrode calibrated with standard buffers at pH 4 and 7 in H₂O and are not corrected for the deuterium isotope effect. ^b At 298 K, in kJ/mol. ^c ΔH° and ΔS° values are average values and have been calculated using the procedure described in the Experimental Section. ^d In J/molK. ^e %S²⁹⁸ values were calculated from the corresponding ΔG° using the relation: %S²⁹⁸ = 100[exp(- $\Delta G^{\circ}/RT$)]/[exp(- $\Delta G^{\circ}/RT$) + 1].

energy (ΔG°) at 298 K of N \rightleftharpoons S pseudorotational equilibrium of **1–13** as a function of pD are presented in Tables 1–8. The signs of the thermodynamic parameters in Tables 1–8 are arbitrarily chosen in such a way that the positive values indicate the drive of N \rightleftharpoons S equilibrium to N, whereas the negative values describe the drive toward S.

The plot of ΔH° , ΔS° (not shown), or ΔG° values of the N \rightleftharpoons S pseudorotational equilibrium of **1–13** as a function of pD displays a sigmoidal dependence characteristic of a typical titration curve for pK_a measurement (Figures 2 and 3). It can be seen from Figures 2–3 that (i) the inflection points of these sigmoidal curves correspond to the pK_a of the heterocyclic base, which has been corroborated by the independent pK_a measurement of the pD dependent ¹H-NMR chemical shift measurements of the aromatic and anomeric protons in **1–13** (Figures 4 and 5) (see section IV) and (ii) the change of electronic nature of the heterocycle from the neutral to the protonated or the deprotonated state is transmittable through the anomeric effect to dictate the N \rightleftharpoons S pseudorotational equilibrium of the pentofuranose moiety of nucleosides (see section V).

(II) The Thermodynamics of pD-Dependent N \rightleftharpoons S Pseudorotational Equilibria of 2'-Deoxyribonucleosides

(a) Comparison of the Energetics of N \rightleftharpoons S Equilibria of the Neutral versus Protonated States of 2'-Deoxyribonucleosides. In 2'-deoxynucleosides **1–6** and dImb **7**, the protonation or deprotonation of the nucleobase modulates exclusively the strength of its anomeric effect which can be observed by monitoring the relative ratio of pseudoaxial (*i.e.*, in N-type conformer) and pseudoequatorial (*i.e.*, in S-type conformer) orientations of the aglycon by the relative ΔH° , ΔS° , and ΔG° values of the pseudorotational equilibrium of the sugar moieties in **1–7**. The values of enthalpy (ΔH°_N), entropy contribution ($-T\Delta S^{\circ}_N$), and free-energy (ΔG°_N), as well as populations of S-type pseudorotamers at 298 K (% S_N²⁹⁸) in the neutral states (the subscript N denotes the neutral state) of **1–7** are presented in Table 8. In the neutral states, negative ΔH°_N values predominate in the drive of the N \rightleftharpoons S equilibrium of the sugar moieties of **1–7** toward S-type conformations over the weaker $-T\Delta S^{\circ}_N$ contributions which oppose the ΔH°_N term by favoring

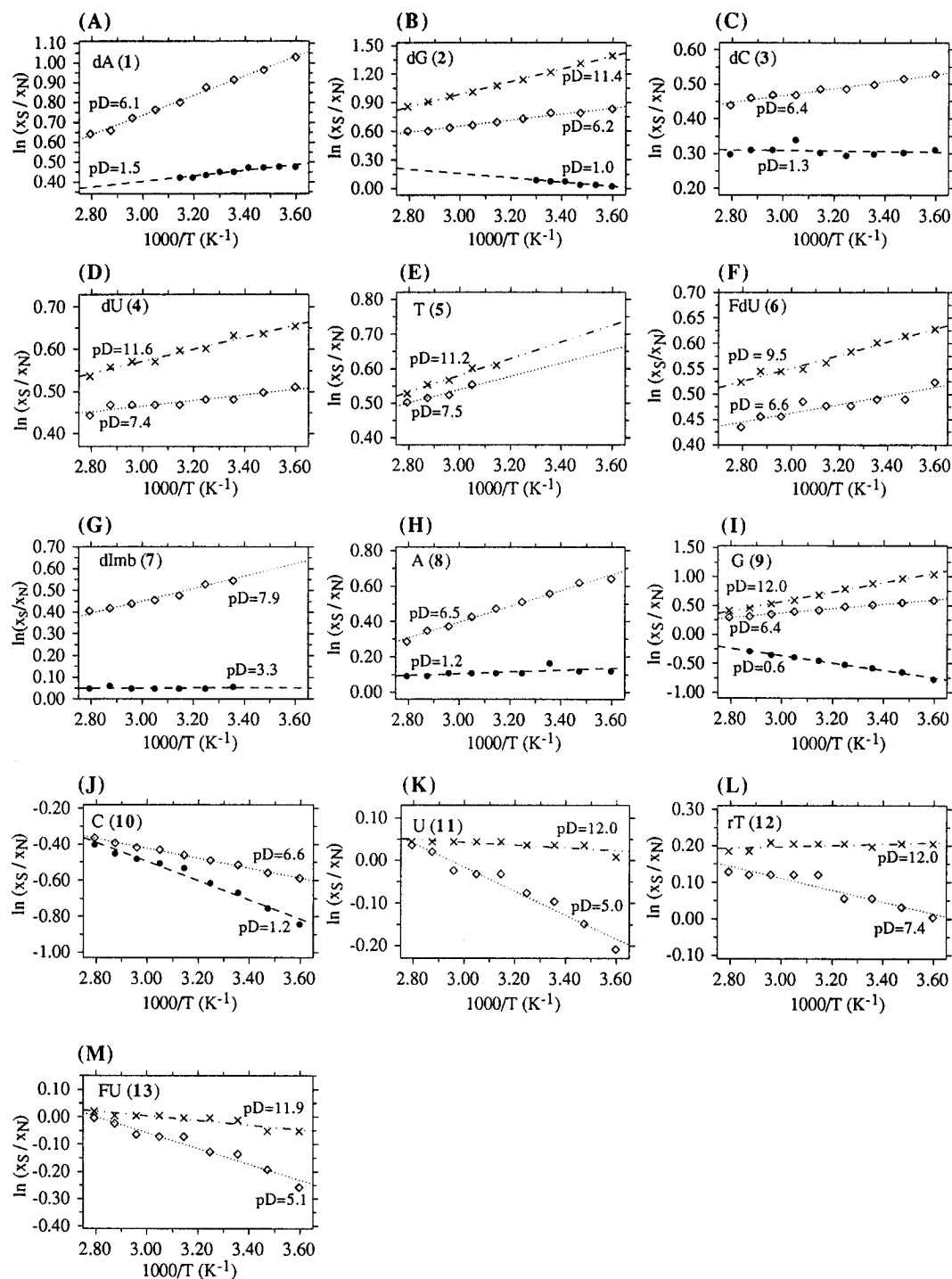


Figure 1. van't Hoff plots of $\ln(x_S/x_N)$ as a function of $1000/T$ in acidic (●, ---), neutral (◇, ...) and alkaline (×, - · - ·) pD region in ca. 0.5 pD unit intervals. The least-squares fitted straight lines are based on the mole fractions of N (x_N) and S (x_S) pseudorotamers in $N \rightleftharpoons S$ pseudorotational equilibrium from PSEUROT analysis of $^3J_{\text{HH}}$ acquired at various temperatures in 278–358 K range for 1–13 (see the Experimental Section). For clarity, only one van't Hoff plot is shown in panels A–M for 1–13 at two or three pD values. (A) The representative van't Hoff plots for dA (1) at pD = 1.5 [●, ---, slope = 0.14 ($\sigma = 0.02$) and an intercept of -0.02 ($\sigma = 0.06$), $R = 0.955$], and pD = 6.1 [◇, ..., slope = 0.50 ($\sigma = 0.01$) and an intercept of -0.75 ($\sigma = 0.04$), $R = 0.998$] (Ψ_m (N) and (S) = 30°). (B) The representative van't Hoff plots for dG (2) at pD = 1.0 [●, ---, slope = -0.22 ($\sigma = 0.03$) and an intercept of 0.83 ($\sigma = 0.1$), $R = 0.959$], at pD = 6.2 [◇, ..., slope = 0.31 ($\sigma = 0.02$) and an intercept of -0.28 ($\sigma = 0.05$), $R = 0.990$], and at pD = 11.4 [×, - · - ·, slope = 0.67 ($\sigma = 0.01$), and an intercept of -1.02 ($\sigma = 0.03$), $R = 0.999$] (Ψ_m (N) and (S) = 30°). (C) The representative van't Hoff plots for dC (3) at pD = 1.3 [●, ---, slope = -0.14 ($\sigma = 0.02$) and an intercept of 0.33 ($\sigma = 0.06$), $R = 0.162$] and pD = 6.4 [◇, ..., slope = 0.10 ($\sigma = 0.01$) and an intercept = 0.17 ($\sigma = 0.02$), $R = 0.983$] (Ψ_m (N) and (S) = 29°). (D) The representative van't Hoff plots for dU (4) at pD = 7.4 [◇, ..., slope = 0.07 ($\sigma = 0.01$) and an intercept of 0.27 ($\sigma = 0.03$), $R = 0.936$] and at pD = 11.6 [×, - · - ·, slope = 0.14 ($\sigma = 0.01$) and an intercept of 0.14 ($\sigma = 0.03$), $R = 0.988$] (Ψ_m (N) and (S) = 35°). (E) The representative van't Hoff plots for T (5) at pD = 7.5 [◇, ..., slope = 0.19 ($\sigma = 0.04$) and an intercept of -0.04 ($\sigma = 0.1$), $R = 0.967$] and at pD = 11.2 [×, - · - ·, slope = 0.24 ($\sigma = 0.03$) and an intercept of -0.14 ($\sigma = 0.07$), $R = 0.984$] (Ψ_m (N) and (S) = 34°). (F) The representative van't Hoff plots for FdU (6) at pD = 6.6 [◇, ..., slope = 0.09 ($\sigma = 0.01$) and an intercept of 0.20 ($\sigma = 0.04$), $R = 0.919$] and at pD = 9.5 [×, - · - ·, slope = 0.13 ($\sigma = 0.01$) and an intercept of 0.16 ($\sigma = 0.02$), $R = 0.988$] (Ψ_m (N) and (S) = 33°). (G) The representative van't Hoff plots for dImb (7) at pD = 3.3 [●, ---, slope = 0.00 ($\sigma = 0.01$) and an intercept of 0.05 ($\sigma = 0.03$), $R = 0.02$] and at pD

Table 3. pH-Dependent Thermodynamics of the Two-State N ⇌ S Equilibrium in dC (3) and C (10)

dC (3)						C (10)					
pD ^a	$\Delta H^{\circ}(\sigma)^{b,c}$	$\Delta S^{\circ}(\sigma)^{c,d}$	$-T\Delta S^{\circ}{}^b$	$\Delta G^{\circ}{}^b$	%S ²⁹⁸ ^e	pD ^a	$\Delta H^{\circ}(\sigma)^{b,c}$	$\Delta S^{\circ}(\sigma)^{c,d}$	$-T\Delta S^{\circ}{}^b$	$\Delta G^{\circ}{}^b$	%S ²⁹⁸ ^e
1.3	0.1 (0.1)	2.8 (0.1)	-0.8	-0.7	57	1.2	4.9 (0.2)	10.2 (1.2)	-3.0	1.9	32
1.9	-0.2 (0.1)	2.0 (0.1)	-0.6	-0.8	58	1.8	5.1 (0.2)	10.8 (1.3)	-3.2	1.9	32
2.2	-0.1 (0.1)	2.2 (0.1)	-0.7	-0.8	57	2.3	5.2 (0.2)	11.2 (1.4)	-3.3	1.9	32
2.6	0.1 (0.1)	2.8 (0.1)	-0.8	-0.7	57	2.8	5.1 (0.3)	11.1 (1.5)	-3.3	1.8	33
3.1	0.0 (0.1)	2.8 (0.1)	-0.8	-0.8	58	3.3	5.1 (0.2)	11.0 (1.4)	-3.3	1.8	32
3.6	0.0 (0.1)	2.7 (0.1)	-0.8	-0.8	58	3.7	4.6 (0.2)	9.7 (1.5)	-2.9	1.7	33
3.8	-0.1 (0.1)	2.4 (0.1)	-0.7	-0.8	58	4.0	4.1 (0.2)	8.1 (1.5)	-2.4	1.7	34
4.1	-0.3 (0.1)	2.4 (0.1)	-0.7	-1.0	60	4.2	3.6 (0.2)	6.5 (1.6)	-1.9	1.7	34
4.3	-0.5 (0.1)	1.8 (0.1)	-0.5	-1.0	60	4.7	2.8 (0.2)	4.3 (1.8)	-1.3	1.5	35
4.5	-0.5 (0.1)	2.1 (0.1)	-0.6	-1.1	61	5.3	2.5 (0.1)	3.3 (1.7)	-1.0	1.5	35
4.8	-0.7 (0.1)	1.6 (0.1)	-0.5	-1.2	62	5.8	2.3 (0.1)	2.8 (1.5)	-0.8	1.5	36
5.2	-0.6 (0.1)	1.9 (0.1)	-0.6	-1.3	62	6.6	2.5 (0.1)	3.5 (1.6)	-1.0	1.5	36
5.7	-0.6 (0.1)	2.1 (0.1)	-0.6	-1.2	62						
6.4	-0.8 (0.1)	1.6 (0.1)	-0.5	-1.3	63						

^a Our pD values are given by a pH meter equipped with a calomel electrode calibrated with standard buffers at pH 4 and 7 in H₂O and are not corrected for the deuterium isotope effect. ^b At 298 K, in kJ/mol. ^c ΔH° and ΔS° values are average values and have been calculated using the procedure described in the Experimental Section. ^d In J/molK. ^e %S²⁹⁸ values were calculated from the corresponding ΔG° using the relation: %S²⁹⁸ = 100[exp(- $\Delta G^{\circ}/RT$)]/[exp(- $\Delta G^{\circ}/RT$) + 1].

Table 4. pH-Dependent Thermodynamics of the Two-State N ⇌ S Equilibrium in dU (4) and U (11)

dU (4)						U (11)					
pD ^a	$\Delta H^{\circ}(\sigma)^{b,c}$	$\Delta S^{\circ}(\sigma)^{c,d}$	$-T\Delta S^{\circ}{}^b$	$\Delta G^{\circ}{}^b$	%S ²⁹⁸ ^e	pD ^a	$\Delta H^{\circ}(\sigma)^{b,c}$	$\Delta S^{\circ}(\sigma)^{c,d}$	$-T\Delta S^{\circ}{}^b$	$\Delta G^{\circ}{}^b$	%S ²⁹⁸ ^e
7.4	-0.6 (0.1)	1.6 (0.8)	-0.5	-1.1	61	5.0	2.1 (0.1)	6.0 (0.9)	-1.8	0.3	47
8.1	-0.7 (0.1)	1.2 (0.8)	-0.4	-1.1	61	7.3	1.9 (0.1)	5.3 (0.9)	-1.6	0.3	47
8.6	-0.8 (0.1)	0.9 (0.9)	-0.3	-1.1	61	7.9	1.8 (0.1)	5.1 (0.9)	-1.5	0.3	47
9.0	-0.8 (0.1)	1.4 (0.9)	-0.4	-1.2	62	8.4	2.0 (0.1)	5.8 (0.8)	-1.7	0.3	47
9.4	-1.0 (0.1)	0.7 (0.9)	-0.2	-1.2	62	8.9	1.6 (0.1)	4.6 (1.0)	-1.4	0.2	48
9.8	-1.2 (0.1)	0.5 (0.9)	-0.1	-1.3	63	9.3	1.4 (0.1)	3.8 (1.0)	-1.1	0.3	47
10.2	-1.2 (0.1)	0.6 (0.8)	-0.2	-1.4	64	9.7	1.0 (0.1)	2.7 (0.9)	-0.8	0.2	48
10.7	-1.3 (0.1)	0.5 (0.8)	-0.1	-1.4	64	10.1	0.8 (0.1)	2.1 (1.1)	-0.6	0.2	48
11.1	-1.3 (0.1)	0.3 (0.8)	-0.1	-1.4	64	10.6	0.6 (0.1)	1.5 (1.1)	-0.5	0.1	49
11.6	-1.2 (0.1)	0.6 (0.8)	-0.2	-1.4	64	11.1	0.5 (0.1)	1.2 (1.1)	-0.4	0.1	49
						11.5	0.3 (0.1)	0.6 (1.1)	-0.2	0.1	49
						12.0	0.2 (0.1)	0.4 (1.0)	-0.1	0.1	49

^a Our pD values are given by a pH meter equipped with a calomel electrode calibrated with standard buffers at pH 4 and 7 in H₂O and are not corrected for the deuterium isotope effect. ^b At 298 K, in kJ/mol. ^c ΔH° and ΔS° are average values calculated using the procedure described in the Experimental Section. ^d In J/molK. ^e %S²⁹⁸ values were calculated from the corresponding ΔG° using the relation: %S²⁹⁸ = 100[exp(- $\Delta G^{\circ}/RT$)]/[exp(- $\Delta G^{\circ}/RT$) + 1].

N-type conformations in dA (1), dG (2), T (5), and dImb (7) but ΔH°_N and $-T\Delta S^{\circ}_N$ contributions act in a cooperative manner in the drive of the pseudorotational equilibria toward S in dC (3), dU (4), and FdU (6) (Table 8). As a result, the N ⇌ S pseudorotational equilibria in 1–7 are controlled by negative ΔG°_N values which correspond to 61–70% S at 298 K (Table 8). A comparison of the relative values of ΔH°_N terms at the neutral pD (Table 8) shows that the relative strengths of the anomeric effects (*i.e.*, combined contribution of stereoelectronic¹ and steric effects¹) of the neutral aglycons in the 2'-deoxynucleosides 1–6 and in 7 are as follows: [dA (-3.9 kJ/

mol) < dG (-2.8 kJ/mol) < dImb (-2.2 kJ/mol) < T (-1.4 kJ/mol) < dC (-0.7 kJ/mol) ≈ dU (-0.6 kJ/mol) ≈ FdU (-0.8 kJ/mol)]. The above ΔH°_N contributions for 1–7 show the balance between the relative strengths of gauche and anomeric effects: the preferred S-type conformations, shown by more negative ΔH°_N , are the result of weaker anomeric effect over the stronger [O4'-C4'-C3'-O3'] gauche effect.¹

Upon the decrease of pD, the N ⇌ S equilibria of 1–3 and 7 are gradually shifted to more N-type conformations (Tables 1–3 and 7) until the complete protonation of the constituent heterocycle is achieved, which is indicated

(Figure 1 contd)

= 7.9 [◇, ..., slope = 0.29 (σ = 0.04) and an intercept of -0.41 (σ = 0.01), R = 0.992] (Ψ_m (N) and (S) = 33°). (H) The representative van't Hoff plots for A (8) at pD = 1.2 [●, ---, slope = 0.05 (σ = 0.02) and an intercept of -0.05 (σ = 0.07), R = 0.639] and pD = 6.5 [◇, ..., slope = 0.45 (σ = 0.02) and an intercept of -0.94 (σ = 0.05), R = 0.995] (Ψ_m (N) and (S) = 38°). (I) The representative van't Hoff plots for G (9) at pD = 0.6 [●, ---, slope = -0.64 (σ = 0.02) and an intercept of 1.56 (σ = 0.08), R = 0.996], at pD = 6.4 [◇, ..., slope = 0.38 (σ = 0.01) and an intercept of -0.76 (σ = 0.04), R = 0.997], and at pD = 12.0 [×, - · - ·, slope = 0.82 (σ = 0.02) and an intercept of -1.88 (σ = 0.06), R = 0.998] (Ψ_m (N) and (S) = 37°). (J) The representative van't Hoff plots for C (10) at pD = 1.2 [●, ---, slope = -0.53 (σ = 0.03) and an intercept of 1.10 (σ = 0.10), R = 0.988] (Ψ_m (N) and (S) = 38°), and pD = 6.6 [◇, ..., slope = -0.28 (σ = 0.01) and an intercept of 0.40 (σ = 0.02), R = 0.998] (Ψ_m (N) and (S) = 36°). (K) The representative van't Hoff plots for U (11) at pD = 5.0 [◇, ..., slope = -0.28 (σ = 0.02) and an intercept of 0.83 (σ = 0.07), R = 0.978] and at pD = 12.0 [×, - · - ·, slope = -0.03 (σ = 0.01) and an intercept of 0.14 (σ = 0.03), R = 0.787] (Ψ_m (N) and (S) = 36°). (L) The representative van't Hoff plots for rT (12) at pD = 7.4 [◇, ..., slope = -0.16 (σ = 0.02) and an intercept of 0.60 (σ = 0.07), R = 0.939] (Ψ_m (N) and (S) = 36°), and at pD = 12.0 [×, - · - ·, slope = 0.02 (σ = 0.01) and an intercept of 0.14 (σ = 0.03), R = 0.546] (Ψ_m (N) and (S) = 35°). (M) The representative van't Hoff plots for FU (13) at pD = 5.1 [◇, ..., slope = -0.29 (σ = 0.02) and an intercept of 0.81 (σ = 0.08), R = 0.976] and at pD = 11.9 [×, - · - ·, slope = -0.08 (σ = 0.01) and an intercept of 0.26 (σ = 0.04), R = 0.916] (Ψ_m (N) and (S) = 35°).

Table 5. pH-Dependent Thermodynamics of the Two-State N \rightleftharpoons S Equilibrium in T (5) and rT (12)

T (5)						rT (12)					
pD ^a	ΔH° (σ) ^{b,c}	ΔS° (σ) ^{c,d}	$-T\Delta S^{\circ}$ ^b	ΔG° ^b	%S ²⁹⁸ ^e	pD ^a	ΔH° (σ) ^{b,c}	ΔS° (σ) ^{c,d}	$-T\Delta S^{\circ}$ ^b	ΔG° ^b	%S ²⁹⁸ ^e
7.5	-1.6 (0.1)	-0.5 (0.3)	0.1	-1.4	64	7.4	1.2 (0.1)	4.6 (0.8)	-1.4	0.2	51
8.3	-1.4 (0.1)	-0.2 (0.3)	0.1	-1.3	63	8.0	1.2 (0.1)	4.4 (0.9)	-1.3	-0.1	51
8.9	-1.3 (0.1)	0.0 (0.4)	0.0	-1.3	63	8.5	1.2 (0.1)	4.4 (0.8)	-1.3	-0.1	51
9.3	-1.6 (0.1)	-0.6 (0.4)	0.2	-1.4	64	9.0	1.1 (0.1)	4.4 (0.7)	-1.3	-0.2	52
9.7	-1.9 (0.1)	-1.5 (0.4)	0.4	-1.4	64	9.5	0.6 (0.1)	2.8 (0.9)	-0.8	-0.2	52
10.0	-1.8 (0.1)	-1.1 (0.5)	0.3	-1.5	64	9.8	0.3 (0.1)	1.9 (1.0)	-0.6	-0.3	53
10.4	-1.9 (0.1)	-1.1 (0.3)	0.3	-1.6	65	10.1	0.1 (0.1)	1.2 (0.9)	-0.4	-0.3	53
11.2	-2.0 (0.1)	-1.4 (0.2)	0.4	-1.6	66	10.5	0.1 (0.1)	1.4 (0.9)	-0.4	-0.3	53
11.9	-1.7 (0.1)	-0.3 (0.2)	0.1	1.6	66	11.0	0.0 (0.1)	0.9 (0.9)	-0.3	-0.3	53
						11.4	0.0 (0.1)	1.0 (1.0)	-0.3	-0.3	53
						12.0	-0.2 (0.1)	0.5 (1.1)	-0.1	-0.3	53

^a Our pD values are given by a pH meter equipped with a calomel electrode calibrated with standard buffers at pH 4 and 7 in H₂O and are not corrected for the deuterium isotope effect. ^b At 298 K, in kJ/mol. ^c ΔH° and ΔS° values are average values and have been calculated using the procedure described in the Experimental Section. ^d In J/molK. ^e %S²⁹⁸ values were calculated from the corresponding ΔG° using the relation: %S²⁹⁸ = 100[exp(- $\Delta G^{\circ}/RT$)]/[exp(- $\Delta G^{\circ}/RT$) + 1].

Table 6. pH-Dependent Thermodynamics of the Two-State N \rightleftharpoons S Equilibrium in FdU (6) and FU (13)

FdU (6)						FU (13)					
pD ^a	ΔH° (σ) ^{b,c}	ΔS° (σ) ^{c,d}	$-T\Delta S^{\circ}$ ^b	ΔG° ^b	%S ²⁹⁸ ^e	pD ^a	ΔH° (σ) ^{b,c}	ΔS° (σ) ^{c,d}	$-T\Delta S^{\circ}$ ^b	ΔG° ^b	%S ²⁹⁸ ^e
4.0	-0.8 (0.1)	1.2 (0.1)	-0.4	1.2	61	5.1	2.3 (0.1)	6.1 (0.7)	-1.8	0.5	45
6.1	-0.8 (0.1)	1.2 (0.1)	-0.4	-1.2	62	6.5	2.3 (0.1)	6.1 (0.8)	-1.8	0.5	45
6.6	-0.7 (0.1)	1.6 (0.1)	-0.5	-1.2	62	7.1	1.9 (0.1)	4.8 (0.7)	-1.4	0.5	45
7.0	-0.8 (0.1)	1.6 (0.1)	-0.5	-1.2	62	7.6	1.9 (0.1)	5.0 (0.8)	-1.5	0.4	46
7.4	-0.8 (0.1)	1.5 (0.1)	-0.4	-1.3	63	8.0	1.4 (0.1)	3.7 (0.9)	-1.1	0.3	47
7.9	-1.0 (0.1)	1.2 (0.1)	-0.3	-1.3	63	8.5	0.9 (0.1)	2.1 (1.1)	-0.6	0.3	47
8.2	-1.2 (0.1)	0.7 (0.2)	-0.2	-1.4	64	9.0	1.0 (0.1)	2.5 (0.9)	-0.7	0.2	47
8.5	-1.1 (0.1)	1.0 (0.2)	-0.3	-1.4	64	9.5	1.0 (0.1)	2.5 (1.0)	-0.7	0.2	47
9.0	-1.2 (0.1)	1.0 (0.2)	-0.3	-1.5	65	10.0	0.9 (0.1)	2.3 (1.0)	-0.7	0.2	48
9.5	-1.1 (0.1)	1.2 (0.2)	-0.4	-1.5	64	10.4	0.8 (0.1)	1.8 (1.0)	-0.5	0.2	47
10.1	-1.1 (0.1)	1.4 (0.2)	-0.4	-1.5	65	10.8	0.8 (0.1)	1.9 (1.0)	-0.6	0.2	48
10.7	-1.1 (0.1)	1.4 (0.1)	-0.4	-1.5	65	11.9	0.6 (0.1)	1.3 (0.9)	-0.4	0.2	48
11.8	-1.0 (0.1)	1.5 (0.2)	-0.4	-1.4	64						

^a Our pD values are given by a pH meter equipped with a calomel electrode calibrated with standard buffers at pH 4 and 7 in H₂O and are not corrected for the deuterium isotope effect. ^b At 298 K, in kJ/mol. ^c ΔH° and ΔS° values are average values and have been calculated using the procedure described in the Experimental Section. ^d In J/molK. ^e %S²⁹⁸ values were calculated from the corresponding ΔG° using the relation: %S²⁹⁸ = 100[exp(- $\Delta G^{\circ}/RT$)]/[exp(- $\Delta G^{\circ}/RT$) + 1].

Table 7. pH-Dependent Thermodynamics of the Two-State N \rightleftharpoons S Equilibrium in dImb (7)

dImb (7)					
pD ^a	ΔH° (σ) ^{b,c}	ΔS° (σ) ^{c,d}	$-T\Delta S^{\circ}$ ^b	ΔG° ^b	%S ²⁹⁸ ^e
2.4	0.2 (0.1)	1.0 (0.1)	-0.3	-0.1	51
3.3	0.0 (0.1)	0.3 (0.1)	-0.1	-0.1	51
5.0	0.1 (0.1)	1.0 (0.1)	-0.3	-0.2	52
5.4	-0.4 (0.1)	-0.1 (0.1)	0.0	-0.4	54
6.0	-0.8 (0.1)	-0.3 (0.1)	0.1	-0.7	57
6.4	-1.3 (0.1)	-1.1 (0.1)	0.3	-1.0	60
6.9	-1.7 (0.1)	-1.7 (0.1)	0.5	-1.2	62
7.9	-2.3 (0.1)	-3.4 (0.2)	1.0	-1.3	63
9.7	-2.3 (0.1)	-3.3 (0.2)	1.0	-1.3	63
10.8	-1.9 (0.1)	-1.8 (0.1)	0.5	-1.4	63

^a Our pD values are given by a pH meter equipped with a calomel electrode calibrated with standard buffers at pH 4 and 7 in H₂O and are not corrected for the deuterium isotope effect. ^b At 298 K, in kJ/mol. ^c ΔH° and ΔS° values are average values and have been calculated using the procedure described in the Experimental Section. ^d In J/molK. ^e %S²⁹⁸ values were calculated from the corresponding ΔG° using the relation: %S²⁹⁸ = 100[exp(- $\Delta G^{\circ}/RT$)]/[exp(- $\Delta G^{\circ}/RT$) + 1].

by unchanged N \rightleftharpoons S equilibria upon the further decrease of pD of the aqueous solution. The values of enthalpy (ΔH°_P) and entropy contribution ($-T\Delta S^{\circ}_P$) to the free-energy (ΔG°_P) as well as populations of S-type pseudorotamers at 298 K (%S²⁹⁸_P) in the fully protonated states of **1–3** and **7** are presented in Table 8 (the subscript P denotes the protonated state). In the case of dG (**2**) and dImb (**7**) the ΔH°_P values are comparable in strength to the opposing $-T\Delta S^{\circ}_P$ terms in the drive of the N \rightleftharpoons S equilibria and the resulting slightly negative ΔG°_P values

correspond to 51% S at 298 K (Table 8). For dA (**1**), ΔH°_P and $-T\Delta S^{\circ}_P$ contributions work in a cooperative manner and result in a negative ΔG°_P which drives the N \rightleftharpoons S pseudorotational equilibrium to S conformations (61% at 298 K, Table 8), whereas the N \rightleftharpoons S pseudorotational equilibrium of dC (**3**) is exclusively controlled in the protonated state by the entropy contribution which results in 58% S at 298 K (Table 8).

The magnitude of the tuning of the anomeric effect in **1–3** and **7** upon protonation of their nucleobases can be easily quantified by a simple comparison of their respective ΔH° , ΔS° , ΔG° , and %N²⁹⁸ values in the protonated versus neutral states (Table 8, Figure 2). The subtraction (*i.e.*, $\Delta\Delta H^{\circ}_{(P-N)}$) of ΔH°_N from ΔH°_P values shows that the preference for N-type conformers (*i.e.*, the preference for the pseudoaxial orientation of the aglycon) has increased by 3.2 kJ/mol for dA (**1**), 4.9 kJ/mol for dG (**2**), 0.7 kJ/mol for dC (**3**), and 2.3 kJ/mol for dImb (**7**). These $\Delta\Delta H^{\circ}_{(P-N)}$ values can be safely attributed to the strengthening of the anomeric effect in **1–3** and **7** as they become fully protonated.

The comparison of ΔH°_N and ΔH°_P values of dG (**2**) with dA (**1**) shows that the anomeric effect in the former is stronger than that of the latter by +1.1 kJ/mol in the neutral state and by +2.8 kJ/mol in the protonated state (Table 8). Similarly, the comparison of ΔH°_N and ΔH°_P values of dG (**2**) and dImb (**7**) shows that the anomeric effect of guanine base is weaker than that of imidazole moiety by -0.6 kJ/mol in the neutral state but it is however stronger in the protonated state by +2.0 kJ/mol

Table 8. Thermodynamic data of the N ⇌ S Pseudorotational Equilibria of 1–13 with Fully Protonated, Neutral, and Fully Deprotonated Nucleobases^a and the Corresponding pK_a Values^b

compd	energetics of N ⇌ S equilibrium when the nucleobase is fully protonated ^a					energetics of N ⇌ S equilibrium when the nucleobase is neutral ^a					energetics of N ⇌ S equilibrium when the nucleobase is fully deprotonated ^a				
	ΔH° _P	ΔS° _P	-TΔS° _P	ΔG° _P	%S _P ²⁹⁸	ΔH° _N	ΔS° _N	-TΔS° _N	ΔG° _N	%S _N ²⁹⁸	ΔH° _D	ΔS° _D	-TΔS° _D	ΔG° _D	%S _D ²⁹⁸
dA (1)	-0.7 (0.1)	1.3 (0.4)	-0.4	-1.1	61	-3.9 (0.2)	-6.1 (0.7)	1.8	-2.1	70	-4.9 (0.2)	-7.4 (0.6)	2.2	-2.7	75
dG (2)	2.1 (0.1)	7.5 (0.6)	-2.2	-0.1	51	-2.8 (0.2)	-3.6 (0.7)	1.1	-1.7	67					
dC (3)	0.0 (0.1)	2.6 (0.3)	-0.8	-0.8	58	-0.7 (0.1)	1.8 (0.2)	-0.5	-1.3	63					
dU (4)						-0.6 (0.2)	1.4 (0.3)	-0.4	-1.1	61					
T (5)						-1.4 (0.2)	-0.4 (0.3)	0.1	-1.3	63					
FdU (6)	0.1 (0.1)	0.7 (0.1)	-0.2	-0.1	51	-0.8 (0.1)	1.4 (0.2)	-0.4	-1.2	62					
dImb (7)						-2.2 (0.1)	-2.8 (0.1)	0.8	-1.4	63					
A (8)	-0.2 (0.1)	1.3 (0.6)	-0.4	-0.5	55	-4.4 (0.2)	-8.7 (0.5)	2.6	-1.8	67					
G (9)	5.4 (0.2)	14.0 (1.7)	-4.2	1.5	35	-3.3 (0.2)	-6.2 (0.7)	1.8	-1.5	65					
C (10)	5.2 (0.2)	11.1 (1.3)	-3.3	1.9	32	2.3 (0.1)	2.8 (1.6)	-0.8	1.5	35					
U (11)						2.0 (0.2)	5.6 (0.9)	-1.7	0.3	47					
rT (12)						1.3 (0.1)	4.6 (0.9)	-1.4	-0.1	51					
FU (13)						2.3 (0.1)	6.0 (0.8)	-1.8	0.5	45					

^a The ΔH°, -TΔS°, and ΔG° are in kJ/mol, all ΔS° are in J/molK. The standard deviations (σ) in ΔH° and ΔS° are in parentheses. The subscripts N, P, and D denote, respectively, the neutral, the protonated, and the deprotonated states. The plateaus in the acidic, neutral, and alkaline ranges for ΔH°, ΔS°, and ΔG° values were obtained by the iterative nonlinear least-squares fitting procedure of the experimental ΔH°, ΔS°, and ΔG° values (Figures 2 and 3) at several pDs (Tables 1–7 for ΔH°, ΔS°, and ΔG° at various pDs for 1–13). ^b The pK_a were calculated through plots of experimental ΔG° of N ⇌ S pseudorotational equilibria at 298 K as a function of pD and the Hill plots of pD as a function of log(ΔΔG°_{tot} - ΔΔG°/ΔΔG°) (Figure S1 in the supporting information). ΔΔG°_{tot} is a total change in ΔG° values between the neutral and the (de)protonated state, whereas ΔΔG° is the change in ΔG° value at a given pD relative to the reference neutral state. The pK_a values were also independently determined from the changes in ¹H-NMR chemical shifts of aromatic and anionic protons in 1–13 at 298 K as a function of pD (Figures 4 and 5): for dA [pK_a = 3.6 from δ(H8), δ(H2), and δ(H1)], see panel A in Figure S1 in the supporting information and its legend for details; for dG [pK_a = 2.2 from δ(H8) and δ(H1)] in the acidic range and pK_a = 9.5 from δ(H8) in the alkaline range, see panels C and D in Figure S1 in the supporting information; for dC [pK_a = 4.3 from δ(H6), δ(H5) and δ(H1)], see panel G in Figure S1 in the supporting information; for dU [pK_a = 9.4 from δ(H6), δ(H5) and δ(H1)], see panel I in Figure S1 in the supporting information; for T [pK_a = 2.2 from δ(H8) and δ(H1)] in the acidic range and pK_a = 9.5 from δ(H8) in the alkaline range, see panels E and F in Figure S1 in the supporting information; for dImb [pK_a = 6.0 from δ(H8) and δ(H1)], see panel K in Figure S1 in the supporting information; for FdU [pK_a = 7.7 from δ(H6), δ(H5) and δ(H1)], see panel M in Figure S1 in the supporting information; for dC [pK_a = 9.8 from δ(H6) and δ(H1)], see panel O in Figure S1 in the supporting information; for dU [pK_a = 3.5 from δ(H8) and δ(H1)] and 3.6 from δ(H2), see panel R in Figure S1 in the supporting information; for dImb [pK_a = 6.0 from δ(Ha), δ(Hb), and δ(Hc)], see panel O in Figure S1 in the supporting information; for A [pK_a = 2.1 from δ(H8) and δ(H1)] in the acidic range and pK_a = 9.4 from δ(H8) and 9.8 from δ(H1) in the supporting information; for C [pK_a = 4.1 from δ(H8) and δ(H1)] in the acidic range and pK_a = 9.4 from δ(H8) and 9.8 from δ(H1) in the supporting information; for U [pK_a = 9.4 from δ(H6) and 9.3 from δ(H5)], see panel c in Figure S1 in the supporting information; for rT [pK_a = 9.8 from δ(H6) and 9.6 from δ(H1)], see panel e in Figure S1 in the supporting information; and for FU [pK_a = 7.6 from δ(H6), see panel g in Figure S1 in the supporting information]. For an independent determination of the pK_as for 1–6 and 8–13, see refs 5 and 11a–c.

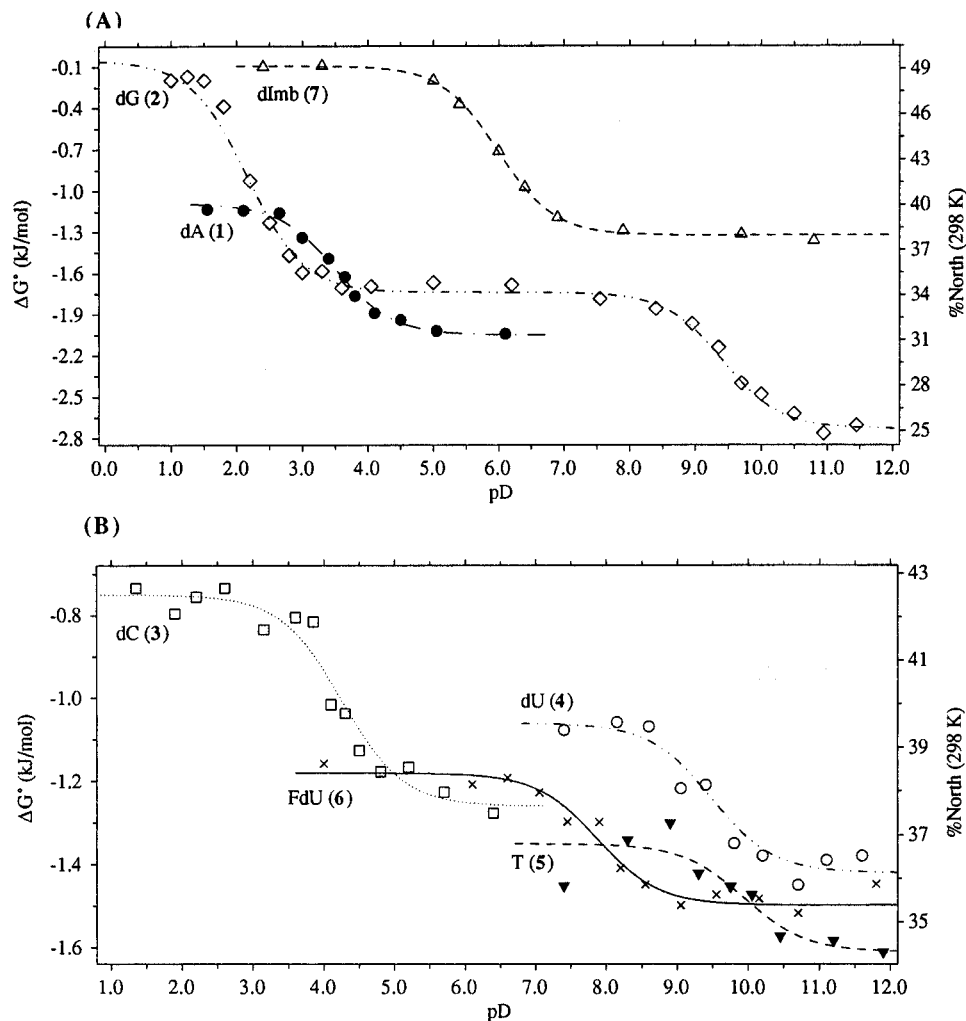


Figure 2. pD-dependent experimental ΔG° values at 298 K for the $N \rightleftharpoons S$ pseudorotational equilibrium of 2'-deoxynucleosides 1–7 determined from van't Hoff plots. (A) The plots of experimental ΔG° values for the $N \rightleftharpoons S$ pseudorotational equilibrium of dA (1) (●, - · - ·) as a function of pDs (Table 1), dG (2) (◇, - · - ·, see Table 2), and dImb (7) (Δ, - - -, Table 7). The sigmoidal curves are the best iterative least-squares fit of the 11 pD-dependent experimental ΔG° values for dA (1), 22 for dG (2), and 10 for dImb (7), giving the pK_a of the nucleobase at the inflection points (Table 8, and see Figure S1 for the determination of the pK_a 's of the nucleobases using Hill plots in the supporting information). (B) The plots of experimental ΔG° values for the $N \rightleftharpoons S$ pseudorotational equilibrium of dC (3) (□, ···) as a function of pD (Table 3), dU (4) (○, - · - ·, Table 4), T (5) (▼, - - -, Table 5), and FdU (6) (×, - , Table 6). The sigmoidal curves are the best iterative least-squares fit of the 14 pD-dependent experimental ΔG° values for dC (3), 10 for dU (4), 9 for T (5), and 13 for FdU (6), giving the pK_a of the nucleobase at the inflection points (Table 8, and Figure S1 for the determination of the pK_a 's of the nucleobases using Hill plots in the supporting information).

(Table 8). Finally, the comparison of ΔH_P^N and ΔH_P^P values of dImb (7) and dA (1) shows that the anomeric effect at the neutral state in dImb (7) is stronger than in dA (1) by +1.7 kJ/mol, but this difference is reduced to +0.8 kJ/mol in the protonated state (Table 8).

(b) What Makes the Purine and Pyrimidine Moieties in Nucleosides So Unique? The subtractions of ΔH_P^N and ΔH_P^P values (*i.e.*, $\Delta\Delta H_P^{(P-N)}$ values) of dImb (7) from those of dA (1) and dG (2) allow us for the first time to delineate the combined steric and stereoelectronic role of the fused pyrimidine moiety in the purine nucleosides in 1 and 2 compared to simple imidazole moiety in 7: (i) They show that adenine and guanine aglycons not only participate actively in intermolecular hydrogen bonding for recognition processes, but they also serve as *unique steric and stereoelectronic units contributing actively in the drive of the two-state $N \rightleftharpoons S$ pseudorotational equilibrium of the constituent pentofuranose moieties through tuning of the anomeric effect.* The stronger anomeric effect of dImb (7) compared to dA (1) and dG (2) in the neutral state is due to the smaller steric bulk^{1k}

of the imidazole moiety in the former resulting in its larger preference for the pseudoaxial orientation (driving the $N \rightleftharpoons S$ pseudorotational equilibrium to N) compared to the fused imidazole in purines. (ii) The comparison of $\Delta\Delta H_P^{(P-N)}$ values for N3-protonated dImb (7) and N1-protonated dA (1) and N7-protonated dG (2) shows that *the strengthening of the anomeric effect in the imidazole nucleoside is smaller than in the purine nucleosides, showing the effect of general electron-withdrawing character of the fused pyrimidine ring on to the imidazole moiety in the purine nucleobases.* This suggests that the electron-density of N9 in dG (2) is more reduced upon protonation than that of N1 in dImb (7) due to the unique deactivating ability of the pyrimidine moiety fused to the imidazole ring in the former (*vide infra*). (iii) The larger enhancement of the anomeric effect upon protonation of dG (2) ($\Delta\Delta H_P^{(P-N)} = +4.9$ kJ/mol) compared to dA (1) ($\Delta\Delta H_P^{(P-N)} = +3.2$ kJ/mol) shows that *the glycosyl N9 is more deactivated in dG (2) than in dA (1) in the acidic medium owing to the different protonation sites of their*

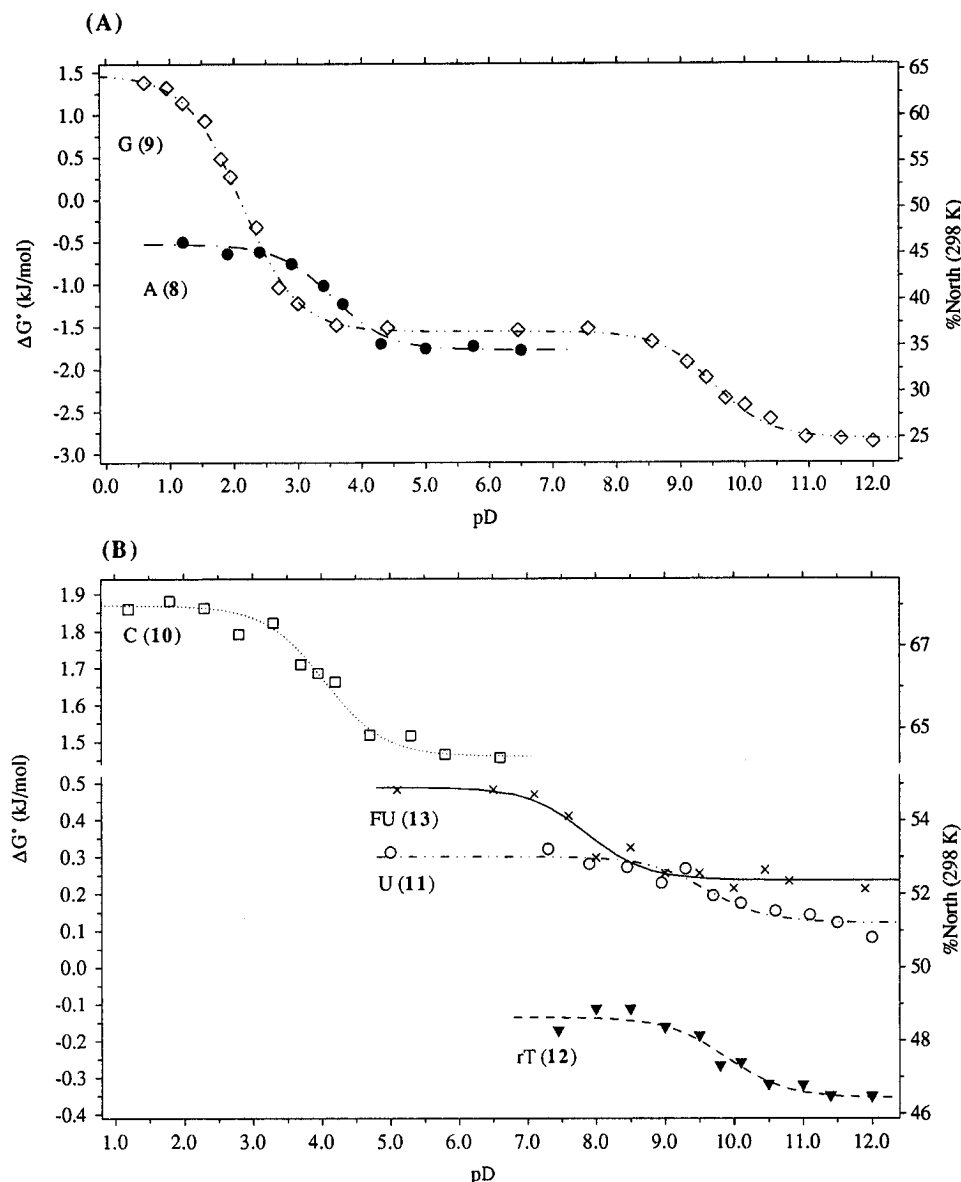


Figure 3. pD-dependent experimental ΔG° values at 298 K for the N \rightleftharpoons S pseudorotational equilibrium of ribonucleosides **8–13** determined from van't Hoff plots. (A) The plots of experimental ΔG° values for the N \rightleftharpoons S pseudorotational equilibrium of A (**8**) (\bullet , - · -) as a function of pD (Table 1) and G (**9**) (\diamond , - · · - , Table 2). The sigmoidal curves are the best iterative least-squares fit of the 10 pD-dependent experimental ΔG° values for A (**8**) and 22 for G (**9**), giving the pK_a of the nucleobase at the inflection points (Table 8, and Figure S1 for the determination of the pK_a 's of the nucleobases using Hill plots in the supporting information). (B) The plots of experimental ΔG° values for the N \rightleftharpoons S pseudorotational equilibrium of C (**10**) (\square , · · ·), U (**11**) (\circ , - · - , Table 4), rT (**12**) (\blacktriangledown , - - -, Table 5), and FU (**13**) (\times , solid -, Table 6). The sigmoidal curves are the best iterative least-squares fit of the 12 pD-dependent experimental ΔG° values for C (**10**), 12 for U (**11**), 11 for rT (**12**), and 12 for FU (**13**), giving the pK_a of the nucleobase at the inflection points (Table 8, and Figure S1 for the determination of the pK_a 's of the nucleobases using Hill plots in the supporting information).

nucleobases (*i.e.*, N7 in the former versus N1 in the latter) (*vide infra*).

(c) The Use of ^{15}N -NMR as a Tool To Understand the Relative Nature of Electron Delocalization in Purines and Pyrimidines. The nature of electron delocalization (Scheme 3) in the aglycons of nucleosides can be qualitatively assessed by the relative ^{15}N -NMR chemical shifts in the neutral versus protonated states of nucleosides, since it offers a simple distinction between their constituent nitrogen atoms: (i) the amino ($\delta \approx -300$ ppm from reference MeNO_2), (ii) the "pyrrole" and "amide" ($\delta \approx -200$ ppm), and (iii) the "azine" or "pyridine" ($\delta \approx -130$ ppm). The larger the deshielding of the glycosyl nitrogen atom in nucleosides, the greater is its azine (sp^2) character. Noteworthy is the comparison of

^{15}N shifts under neutral condition amongst adenosine (-205.6 ppm) and guanosine (-205.3 ppm) and with those of cytidine (-222.2 ppm), uridine (-231.6 ppm), and ribothymidine (-231.3 ppm)].¹⁰ These ^{15}N -NMR data show that the sp^2 or the azine character of the "pyrrole-type" glycosyl nitrogen increases in the following order: uracil \approx thymine $<$ cytosine \ll adenine \approx guanine. This shows that the observed weakening of the anomeric effect from pyrimidines to purines can be qualitatively correlated to the relative strengths of the azine character of their "pyrrole-type" glycosyl nitrogens in the neutral medium.

Upon protonation of guanosine, the delocalization of the lone-pair of glycosyl N^9 stabilizes the N^7H^+ species A (see Scheme 3) to give the partly positively charged

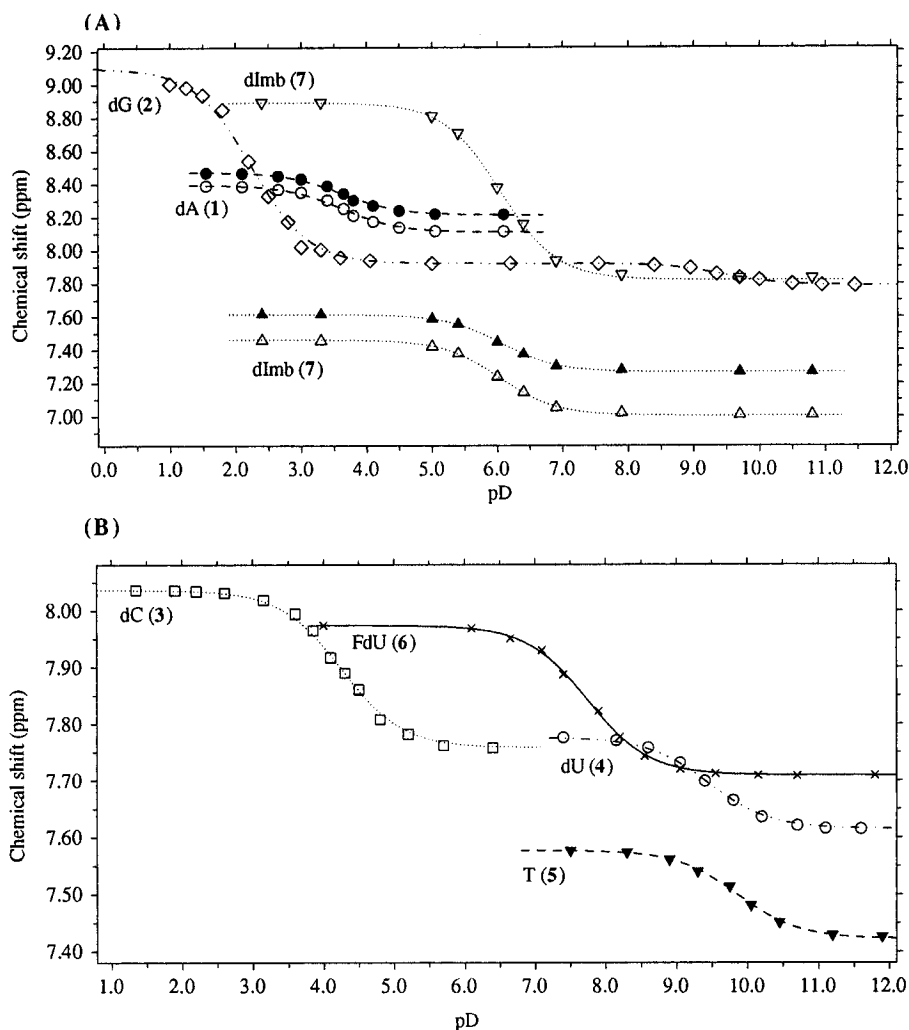


Figure 4. pH-dependent ¹H chemical shifts of the aromatic protons of the nucleobase in 2'-deoxynucleosides 1–7. (A) The plots of the pH-dependent ¹H chemical shifts at 298K of H8 (●, ---) and H2 (○, ---) for dA (1) (11 different pD values from 1.5 to 6.1 at ca. 0.5 pD unit intervals), of H8 (◇, - · - ·) for dG (2) (22 different pD values from 1.0 to 11.4 at ca. 0.5 pD unit intervals), and of Ha (Δ, ···), Hb (▲, ···) and Hc (▽, ···) for dImb (7) (10 different pD values from 2.4 to 10.8 at ca. 0.5 pD unit interval), showing the sigmoidal curves. These sigmoidal curves are the best iterative least-squares fit of the 11 pD-dependent experimental chemical shifts for dA (1), 22 for dG (2), and 10 for dImb (7) (eq 1), giving the p*K*_a of the nucleobases at the inflection points (Table 8, and Figure S1 for the determination of the p*K*_a's of the nucleobases using Hill plots in the supporting information). (B) The plots of the pH-dependent ¹H chemical shifts at 298K of H6 (□, ···) for dC (3) (14 different pD values from 1.3 to 6.4 at ca. 0.5 pD unit intervals), of H6 (○, - · - ·) for dU (4) (10 different pD values from 7.4 to 11.6 at ca. 0.5 pD unit intervals), of H6 (▼, - - -) for T (5) (9 different pD values from 7.5 to 11.9 at ca. 0.5 pD unit interval) and of H6 (×, solid -) for FdU (6) (13 different pD values from 4.0 to 11.8 at ca. 0.5 pD unit interval) showing the sigmoidal curves. These sigmoidal curves are the best iterative least-squares fit of the 14 pD-dependent experimental chemical shifts for dC (3), 10 for dU (4), 9 for T (5) (eq 1), and 13 for FdU (6), giving the p*K*_a of the nucleobases at the inflection points (Table 8, and Figure S1 for the determination of the p*K*_a's of the nucleobases using Hill plots in the supporting information).

N⁹ (B), which has a certain azine character, explaining its downfield shift by 6.7 ppm.⁹ In B, the conjugation of 2-aminopyrimidone moiety leads to C which is itself in a tautomeric equilibrium with D. Note that the ¹⁵N chemical shift of N7 of guanosine (−133.9 ppm) shifts to −179.9 ppm upon protonation,^{9b} whereas N⁷ and N⁹ for inosine absorb at −131.9 and at −206.6 ppm at neutral pH, which upon protonation shifts to −141.2 ppm and −205.6 ppm, respectively.⁹ Thus, the comparison of the observed $\Delta\delta^{15}\text{N7}$ of guanosine (46 ppm) and inosine (10.3 ppm) and their effects on their respective “pyrrole-type” glycosyl nitrogen [$\Delta\delta^{15}\text{N9}$ of guanosine (6.7 ppm) and inosine (1.0 ppm)] in the acidic medium shows the relative deactivating power of the respective fused pyrimidone ring exerted on the π -electron rich fused imidazole.

The ¹⁵N chemical shift of N3 of 1-methylimidazole (−128.5 ppm) shifts to −203.6 ppm upon protonation

($\Delta\delta^{15}\text{N3} = 75.1$ ppm), showing that its “azine” character is more pronounced than that of guanosine¹⁵ because of absence of fused deactivating pyrimidine moiety. The delocalization of the N1 lone pair in E results in a partial positive charge on N1 in F, explaining the 7.4 ppm downfield shift of N1 upon N3 protonation.

Similarly, delocalization of the N9 lone pair in adenosine to stabilize the N¹H⁺ in G results in partly positively charged N⁹ with a partial “azine-type” character in H which can be further delocalized into I, resulting in its downfield shift by 6.6 ppm upon protonation. In cytidine, the lone pair of glycosyl N¹ in J is already involved in the “amide-type” resonance form K even in the neutral state, and the nature of this conjugation is hardly affected upon protonation at N³, which is experimentally evi-

(15) Schuster, I.; Roberts, J. D. *J. Org. Chem.* **1979**, *44*, 3864.

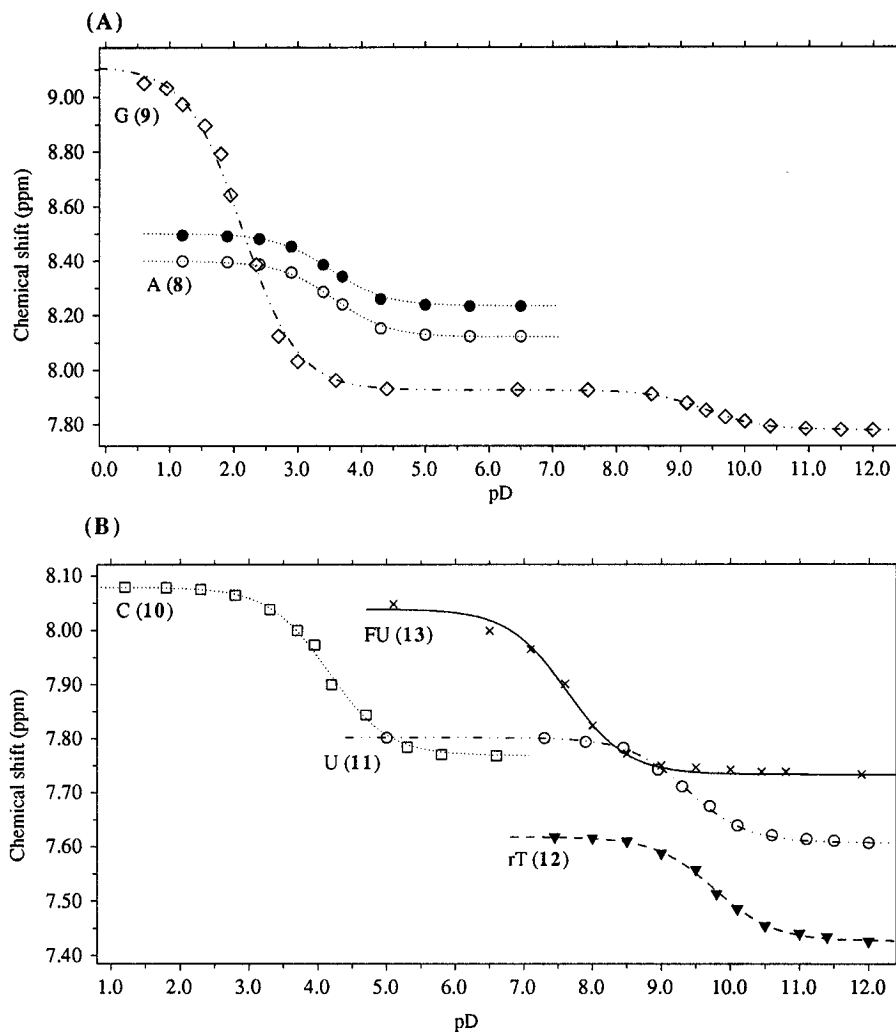


Figure 5. pH-dependent ^1H chemical shifts of the aromatic protons of the nucleobase in ribonucleosides **8**–**13**. (A) The plots of the pH-dependent ^1H chemical shifts at 298K of H8 (●, ---) and H2 (○, ---) for A (**8**) (10 different pD values from 1.2 to 6.5 at ca. 0.5 pD unit intervals), of H8 (◇, - - -) for G (**9**) (22 different pD values from 0.6 to 12.0 at ca. 0.5 pD unit intervals), showing the sigmoidal curves. These sigmoidal curves are the best iterative least-squares fit of the 10 pD-dependent experimental chemical shifts for A (**8**), 22 for G (**9**) (eq 1), giving the $\text{p}K_a$'s of the nucleobases at the inflection points (Table 8, and Figure S1 for the determination of the $\text{p}K_a$'s of the nucleobases using Hill plots in the supporting information). (B) The plots of the pH-dependent ^1H chemical shifts at 298K of H6 (□, ---) for C (**10**) (12 different pD values from 1.2 to 6.6 at ca. 0.5 pD unit intervals), of H6 (○, - - -) for U (**11**) (12 different pD values from 5.0 to 12.0 at ca. 0.5 pD unit intervals), of H6 (▼, - - -) for rT (**12**) (11 different pD values from 7.4 to 12.0 at ca. 0.5 pD unit interval) and of H6 (×, solid —) for FU (**13**) (12 different pD values from 5.1 to 11.9 at ca. 0.5 pD unit interval) showing the sigmoidal curves. These sigmoidal curves are the best iterative least square fit (eq 1) of the 12 pD-dependent experimental chemical shifts for C (**10**), 12 for U (**11**), 11 for rT (**12**), and 12 for FU (**13**), giving the $\text{p}K_a$'s of the nucleobases at the inflection points (Table 8, and Figure S1 for the determination of the $\text{p}K_a$'s of the nucleobases using Hill plots in the supporting information).

denced by the negligible 1.1 ppm downfield shift of this resonance from neutral to protonated cytidine, thereby showing the limited contributions of canonical structures L–N.

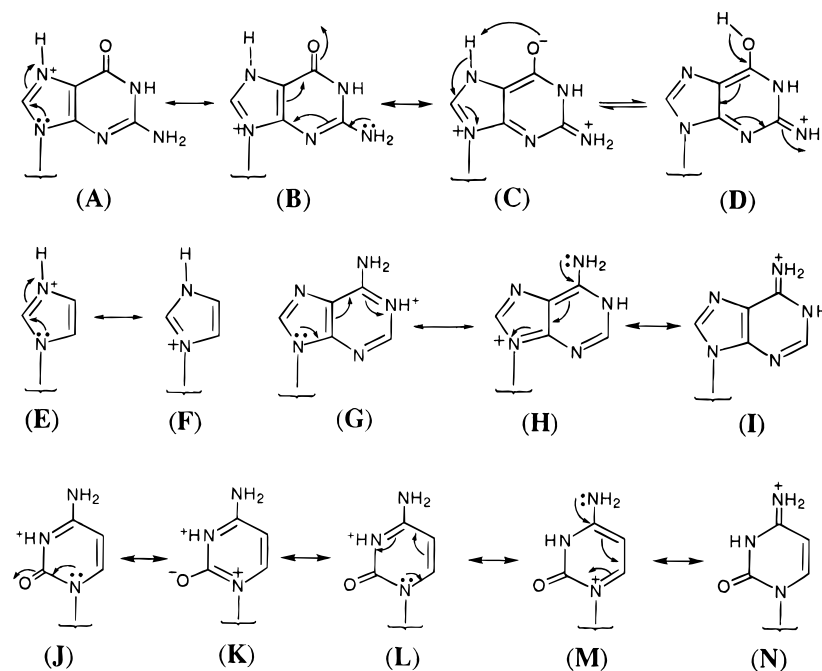
(d) Comparison of the Energetics of $N \rightleftharpoons S$ Equilibria of the Neutral versus Deprotonated States of 2'-Deoxyribonucleosides. Upon the deprotonation of N1 in dG (**2**) and N3 in dU (**4**), T (**5**), and FdU (**6**) at the alkaline pH, their $N \rightleftharpoons S$ equilibria are shifted toward S-type conformations which is reflected in the decrease of their ΔH° , ΔS° , and ΔG° values (see Tables 2 and 4–6). The values of enthalpy (ΔH°_D) and entropy ($-T\Delta S^\circ_D$) contributions to the free-energy (ΔG°_D) as well as populations of S-type pseudorotamers at 298 K ($\%S_D^{298}$) in the fully deprotonated states in dG (**2**), dU (**4**), T (**5**), and FdU (**6**) under the highly alkaline conditions are presented in Table 8 (the subscript D denotes the deprotonated state). The large negative ΔH°_D values

drive the $N \rightleftharpoons S$ equilibrium in dG (**2**), dU (**4**), T (**5**), and FdU (**6**) toward S-type conformations and largely predominate over the weaker $-T\Delta S^\circ_D$ contributions (Table 8). As a result, the $N \rightleftharpoons S$ pseudorotational equilibria in dG (**2**), dU (**4**), T (**5**) and FdU (**6**) are characterized by negative ΔG°_D values which correspond to 62–75% S at 298 K (Table 8).

The subtraction (*i.e.*, $\Delta\Delta H^\circ_{(N-D)}$) of ΔH°_D values for $N \rightleftharpoons S$ pseudorotational equilibria from the corresponding values in the neutral state (ΔH°_N) shows that the preference for the N-type conformers has decreased by $\Delta\Delta H^\circ_{(N-D)}$ of 2.1 kJ/mol for dG (**2**), 0.7 kJ/mol for dU (**4**), 0.5 kJ/mol for T (**5**), and 0.3 kJ/mol for FdU (**6**) due to the weaker anomeric effect in the deprotonated state (Table 8).

One other interesting point that emerges from the comparison of $\Delta\Delta H^\circ_{(P-N)}$ and $\Delta\Delta H^\circ_{(N-D)}$ values (*vide supra*) for dG (**2**) is that owing to the different stereo-

Scheme 3



chemical location of the protonation (N7) and deprotonation (N1) sites from glycosyl N9, the magnitude of $\Delta\Delta H^{\circ}_{(N-D)}$ for the weakening of the anomeric effect (2.1 kJ/mol more preference for the pseudoequatorial orientation of guanine) in the alkaline medium is considerably less than the strengthening of the anomeric effect in the acidic medium ($\Delta\Delta H^{\circ}_{(P-N)} = 4.9$ kJ/mol more preference for the pseudoaxial orientation of guanine). This means that the electronic character of N9 is influenced more strongly by protonation at N7 than by deprotonation at N1.

(III) The Thermodynamics of pD-Dependent N \rightleftharpoons S Pseudorotational Equilibria of Ribonucleosides

(a) Comparison of the Energetics of N \rightleftharpoons S Equilibria of the Neutral versus Protonated States of Ribonucleosides. We have previously shown that the specific nature of glycosyl nitrogen in ribonucleosides **8–12** controls N \rightleftharpoons S pseudorotational equilibria of the constituent sugar moieties both by the distinct anomeric effect and the competing gauche effect of the [N–C1'–C2'–O2'] fragment.¹ We have also shown previously that the strength of the gauche effect in [N_(purine)–C1'–C2'–O2'] and [N_(pyrimidine)–C1'–C2'–O2'] fragments, both of which drive the pseudorotational equilibrium toward S-type conformations, are different in purine and pyrimidine ribonucleosides.¹ Therefore, the protonation or deprotonation of the particular heterocyclic nucleobase in **8–13** will either reinforce or weaken the strength of the intrinsic anomeric and [N–C1'–C2'–O2'] gauche effects because of the change of electronic character of the glycosyl nitrogen. The differences observed in ΔH° , ΔS° , and ΔG° values of the N \rightleftharpoons S pseudorotational equilibria in **8–13** at different pD values (see Tables 1–6) reflect the combined changes in the drive toward the N-type conformers by the anomeric effect and toward the S-type by the [N–C1'–C2'–O2'] gauche effects.

The values of enthalpy (ΔH°_N), entropy contribution ($-T\Delta S^{\circ}_N$), and free-energy (ΔG°_N) of N \rightleftharpoons S equilibria as

well as populations of S-type pseudorotamers at 298 K ($\%S_N^{298}$) in the neutral states of **8–13** are given in Table 8. In the neutral states, ΔH°_N values predominate in the drive of the N \rightleftharpoons S equilibrium of A (**8**) and G (**9**) toward S-type conformations over the weaker entropy contributions ($-T\Delta S^{\circ}_N$) which oppose ΔH°_N term by favoring N-type (Table 8). As a result, the N \rightleftharpoons S pseudorotational equilibria in purine ribonucleosides **8** and **9** are controlled by negative ΔG°_N values which correspond to 67 and 65% S at 298 K (Table 8). In the case of C (**10**), U (**11**), rT (**12**), and FU (**13**) enthalpy drives the N \rightleftharpoons S equilibria in the neutral state toward N-type conformers (*i.e.*, positive ΔH°_N values) and is opposed by the entropy term which is driving toward S-type conformers (Table 8).

The decrease of pD causes the shift of the N \rightleftharpoons S equilibria of **8–10** to more N-type conformation (Tables 1–3) until the complete protonation of the constituent heterocycle is achieved and N \rightleftharpoons S equilibria reach the plateau at the acidic pD values (Table 8). In the fully protonated state N \rightleftharpoons S pseudorotational equilibria of A (**8**), G (**9**), and C (**10**) are characterized by ΔH°_P values which are more positive in comparison with the corresponding ΔH°_N values in the neutral state (Table 8). The shift toward more N-type conformations in **8–10** upon complete protonation, signifying relatively more energetic preference for the pseudoaxially oriented aglycon, can be quantified by the subtraction (*i.e.*, $\Delta\Delta H^{\circ}_{(P-N)}$) of ΔH°_N values in the neutral state from the values in the protonated state (ΔH°_P) which shows that the preference for the pseudoaxially oriented conformers has increased by 4.2 kJ/mol for A (**8**), 8.7 kJ/mol for G (**9**), and 2.9 kJ/mol for C (**10**). This $\Delta\Delta H^{\circ}_{(P-N)}$ values represent the overall changes in the strength of the anomeric preference of the nucleobase owing to the competing strengths of its anomeric and gauche effects of [N–C1'–C2'–O2'] and [O4'–C1'–C2'–O2'] fragments.

The comparison of the $\Delta\Delta H^{\circ}_{(P-N)}$ values for dA (**1**), dG (**2**), and dC (**3**) (*vide supra*) and the corresponding values in A (**8**), G (**9**), and C (**10**), respectively, show that the increase in the preference for the N-type conformers, and hence the pseudoaxially oriented nucleobase, is much

larger in ribo analogs [by 1.0 kJ/mol for dA/A pair, 3.8 kJ/mol for dG/G pair, and 2.2 kJ/mol for dC/C pair; see Table 8], which can be attributed to the gauche effects of both N-C1'-C2'-O2' and O4'-C1'-C2'-O2' fragments.

(b) Comparison of the Energetics of N \rightleftharpoons S Equilibria of the Neutral versus Deprotonated States of Ribonucleosides. Upon deprotonation, the N \rightleftharpoons S equilibria in G (**9**), U (**11**), rT (**12**), and FU (**13**) are shifted toward S-type conformations which is reflected in the decrease of ΔH° , ΔS° , and ΔG° values (Tables 2, and 4–6). The large negative ΔH°_D value in the fully deprotonated state drives the N \rightleftharpoons S equilibrium in G (**9**) toward S-type conformations and predominates over the weaker $-T\Delta S^\circ_D$ contributions (Table 8). In the case of U (**11**), rT (**12**), and FU (**13**), ΔH°_D and $-T\Delta S^\circ_D$ contributions are of comparable strength (Table 8). The subtraction (*i.e.*, $\Delta\Delta H^\circ_{(N-D)}$) of ΔH°_D values from the corresponding values in the neutral state (ΔH°_N) shows that the energetic preference for the pseudoaxial orientation of the aglycon (as evident by the decrease of N-type conformer population) has weakened by $\Delta\Delta H^\circ_{(N-D)}$ of 4.3 kJ/mol for G (**9**), 1.7 kJ/mol for U (**11**), 1.5 kJ/mol for rT (**12**), and 1.5 kJ/mol for FU (**13**).

In summary, a perusal of our data in Table 8 shows that the strength of the anomeric effect in 2'-deoxynucleosides **1–6** and dImb **7** can be modulated upon protonation ($\Delta\Delta H^\circ_{(P-N)}$) or deprotonation ($\Delta\Delta H^\circ_{(N-D)}$) with an increasing efficiency in the following order: thymine \approx uracil \approx 5-fluorouracil \approx cytosine < imidazole < adenine < guanine. The modulation of the drive toward N-type conformers upon protonation ($\Delta\Delta H^\circ_{(P-N)}$) or toward S-type conformers upon deprotonation ($\Delta\Delta H^\circ_{(N-D)}$) in ribonucleosides **8–13** increases in the following order: thymine \approx uracil \approx 5-fluorouracil < cytosine < adenine < guanine (Table 8).

(IV) Determination of pK_a Values from the pD-Dependent Thermodynamics of the Two-State N \rightleftharpoons S Pseudorotational Equilibria and Their Comparison with the pK_a Values Determined from the Analysis of pD-Dependent $\Delta\delta$ of $^1\text{H-NMR}$ Chemical Shifts

The plots of ΔG° values of the N \rightleftharpoons S pseudorotational equilibrium of **1–13** as a function of pD are presented in Figures 2 and 3. The curves through the experimental points were fitted with the use of nonlinear least-squares fitting procedure to the Henderson–Hasselbalch (eq 1)

$$\text{pD} = pK_a + \log \frac{[\text{A}]}{[\text{AH}^+]} = pK_a + \log \frac{(1 - \alpha)}{\alpha} \dots (1)$$

where α is calculated from the change in ΔH° , ΔS° , and ΔG° values relative to the reference neutral state at a given pD divided by the total change in their respective values between the neutral and the protonated or the deprotonated state ($\Delta\Delta H^\circ_{\text{tot}}$, $\Delta\Delta S^\circ_{\text{tot}}$, and $\Delta\Delta G^\circ_{\text{tot}}$). The pK_a values for **1–13** were determined through Hill plots of pD *versus* the logarithm of the ratio of the protonated to the unprotonated species (Figure S1 in the supporting information). Linear regression has given straight lines with the Pearson's correlation coefficients (R) above 0.9 and the slopes close to 1, which is characteristic indication for the protonation involving a single protonation site, and pK_a values were obtained at the intercepts (Figure S1 in the supporting information).

The pK_a values in **1–13** were also independently determined by monitoring the $^1\text{H-NMR}$ chemical shifts of the nonexchangeable aromatic and anomeric protons as a function of the change of pD of the solution at 298 K in the usual manner (Figure S1 in the supporting information). Note that the pK_a values calculated from the thermodynamic parameters of N \rightleftharpoons S pseudorotational equilibria in **1–13** and the pK_a 's from $\Delta\delta$ in $^1\text{H-NMR}$ resonances chemical shifts are virtually identical and correspond to the literature values (± 0.3 pK_a units).^{5,11a-c}

(V) Correlation of Protonation \rightleftharpoons Deprotonation Equilibrium of the Aglycon with the Two-State N \rightleftharpoons S Pseudorotational Equilibrium of the Sugar in Nucleoside

It has been found that the plots of $\delta(^1\text{H})$ as a function of ΔG° of N \rightleftharpoons S pseudorotational equilibria in **1–13** give straight lines (see Figure 6). The Pearson correlation coefficient (R) for the linear relationship between $\delta(^1\text{H})$ *versus* ΔG° of N \rightleftharpoons S pseudorotational equilibria in **1–13** in Figure 6 was found to be larger than 0.97 for all nucleosides, except for T (**5**, $R = 0.90$) and U (**11**, $R = 0.95$) because of the errors involved in the determination of ΔG° for **5** and **11** due to the smaller variation of $^3J_{\text{HH}}$ over the temperature range studied (Tables S4 and S5 in the supporting information). The direct correlation of protonation \rightleftharpoons deprotonation equilibrium of the aglycon with the two-state N \rightleftharpoons S pseudorotational equilibrium of the sugar in various nucleosides found in this work means that the force driving the protonation \rightleftharpoons deprotonation equilibrium of the heterocycle is also transmitted through the anomeric effect to drive the two-state N \rightleftharpoons S pseudorotational equilibrium.

Conclusions

The protonation of nucleobases directly affects their hydrogen-bonding capabilities, thereby affecting the overall three-dimensional structure in deoxyribo- and ribonucleo(s)itides.^{16a-e} This is the first thermodynamic study on how the protonation or the deprotonation of nucleobases dictates the change in the sugar conformation.^{16f} The results and the implications of our studies can be summarized as follows:

(1) This is the first report that quantifies the influence of the pD on the strength of the anomeric effect in the nucleosides and on how it modulates the intrinsic bias of the two-state N \rightleftharpoons S pseudorotational equilibrium of their sugar moieties. The experimental data reported herein have unequivocally and independently proven that the dynamic two state N \rightleftharpoons S conformational model is a valid concept for nucleosides in aqueous solution over a pD range from 0.6 to 12.0. Note that in the earlier works,¹ two state dynamic N \rightleftharpoons S pseudorotational equilibrium in nucleosides was mainly based on statistical distributions of X-ray crystal structures. This was also further corroborated by the NMR observations of two distinctly identifiable and dynamically interconverting

(16) (a) Gao, X.; Patel, D. J. *J. Am. Chem. Soc.* **1988**, *110*, 5178. (b) Dolinnaya, N. G.; Fresco, J. R. *Proc. Natl. Acad. Sci. U.S.A.* **1992**, *89*, 9242. (c) Robinson, H.; van der Marel, G. A.; van Boom, J. H.; Wang, A. H. J. *Biochemistry* **1992**, *31*, 10510. (d) Boulard, Y.; Cognet, J. A. H.; Gabarro-Arpa, J.; Le Bret, M.; Sowers, L. C.; Fazakerley, G. V. *Nucl. Acids Res.* **1992**, *20*, 1933. (e) Jaishree, T. N.; Wang, H.-J. *Nucl. Acids Res.* **1993**, *21*, 3839. (f) Hruska, F. E.; Wood, D. J.; Singh, H. *Biochem. Biophys. Acta* **1977**, *474*, 129.

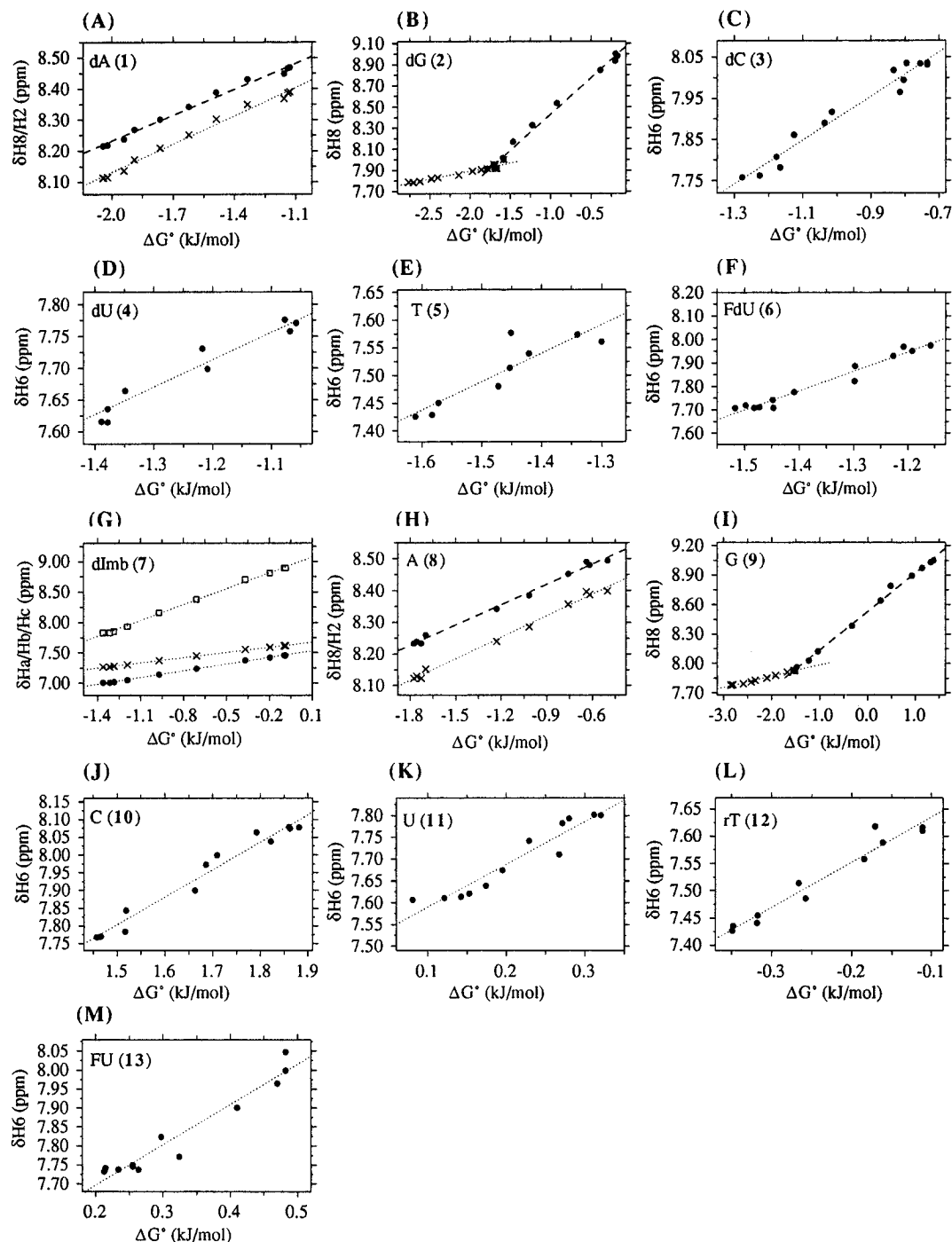


Figure 6. Plots of the correlation of the pD-dependent ^1H -NMR chemical shifts (data not shown) as a function of pD-dependent ΔG° for the $\text{N} \rightleftharpoons \text{S}$ pseudorotational equilibrium at 298 K (Tables 1–7) for 1–13 showing straight lines with different slopes (S), intercepts (I), and correlation coefficients (R). (A) The plots of δH8 (\bullet) and δH2 (\times) for dA (1) at 11 pDs [for H8: $R = 0.995$, $S = 0.28$ ($\sigma = 0.01$), $I = 8.79$ ($\sigma = 0.02$), $I = 8.74$ ($\sigma = 0.02$)]. (B) The plot of δH8 for dG (2) at 14 pDs from 1.0–7.5 (labeled by \bullet) [$R = 0.996$, $S = 0.69$ ($\sigma = 0.02$), $I = 9.12$ ($\sigma = 0.02$)] and from 5.0 to 11.45 (labeled by \times) [$R = 0.994$, $S = 0.13$ ($\sigma < 0.01$), $I = 8.14$ ($\sigma = 0.01$)]. (C) The plot of δH6 (\bullet) for dC (3) at 14 pDs [$R = 0.982$, $S = 0.53$ ($\sigma = 0.03$), $I = 8.44$ ($\sigma = 0.03$)]. (D) The plot of δH6 (\bullet) for dU (4) at 10 pDs [$R = 0.972$, $S = 0.43$ ($\sigma = 0.04$), $I = 8.23$ ($\sigma = 0.05$)]. (E) The plot of δH6 (\bullet) for T (5) at 9 pDs [$R = 0.897$, $S = 0.5$ ($\sigma = 0.1$), $I = 8.3$ ($\sigma = 0.1$)]. (F) The plot of δH6 (\bullet) for FdU (6) at 13 pDs [$R = 0.982$, $S = 0.825$ ($\sigma = 0.05$), $I = 8.94$ ($\sigma = 0.07$)]. (G) The plots of δHa (\bullet), δHb (\times), δHc (\square) at 298 K for dImb (7) at 10 pDs [for Ha: $R = 0.999$, $S = 0.37$ ($\sigma = 0.01$), $I = 7.50$ ($\sigma = 0.01$); for Hb: $R = 0.999$, $S = 0.28$ ($\sigma = 0.01$), $I = 7.65$ ($\sigma = 0.01$). For Hc: $R = 0.999$, $S = 0.87$ ($\sigma = 0.01$), $I = 8.99$ ($\sigma = 0.01$)]. (H) The plots of δH8 (\bullet) and δH2 (\times) for A (8) at 10 pDs [For H8: $R = 0.997$, $S = 0.21$ ($\sigma < 0.01$), $I = 8.61$ ($\sigma < 0.01$). For H2: $R = 0.997$, $S = 0.23$ ($\sigma < 0.01$), $I = 8.53$ ($\sigma < 0.01$)]. (I) The plot of δH8 for G (9) at 13 pDs from 0.6 to 7.5 (labeled by \bullet) [$R = 0.999$, $S = 0.39$ ($\sigma < 0.01$), $I = 8.53$ ($\sigma < 0.01$)] and from 4.4 to 12.0 (labeled by \times) [$R = 0.995$, $S = 0.12$ ($\sigma < 0.01$), $I = 8.10$ ($\sigma < 0.01$)]. (J) The plot of δH6 (\bullet) for C (10) at 12 pDs [$R = 0.982$, $S = 0.77$ ($\sigma = 0.05$), $I = 6.64$ ($\sigma = 0.08$)]. (K) The plot of δH6 (\bullet) for U (11) at 12 pDs [$R = 0.954$, $S = 1.0$ ($\sigma = 0.1$), $I = 7.49$ ($\sigma = 0.02$)]. (L) The plot of δH6 (\bullet) for rT (12) at 11 pDs [$R = 0.975$), $S = 0.83$ ($\sigma = 0.06$), $I = 7.72$ ($\sigma = 0.02$)]. (M) The plot of δH6 (\bullet) for FU (13) at 12 different pDs [$R = 0.968$, $S = 1.06$ ($\sigma = 0.09$), $I = 7.49$ ($\sigma = 0.03$)].

N and S conformations (as evident by their respective chemical shifts and $^3J_{\text{HH}}$) of the constituent sugar moieties in oligonucleotides as in $B \rightleftharpoons Z$ DNA¹⁷ or $A \rightleftharpoons Z$ RNA¹⁸ or in the A-form \rightleftharpoons B-form lariat RNA,¹⁹ despite the fact that the sugar conformation in oligonucleotides is not only controlled by the inherent stereoelectronic intramolecular forces in the nucleoside but also by the energetically important internucleotidyl interactions.

(2) The protonation (or deprotonation) of the nucleobase in nucleosides results in an increased (or decreased) shift of the $N \rightleftharpoons S$ pseudorotational equilibrium toward N conformations, showing the interdependency of change of electronic nature of the nucleobases with the dynamic conformational characteristics of the constituent pentose sugar through the change of the strength of the anomeric effect. The pD dependent modulation of the anomeric effect in the D₂O solution appeared to be less efficient in deoxyribo- than in ribonucleosides, which has been attributed to the specific role of 2'-OH function in the latter compounds.

(3) The comparison of our thermodynamic data on the $N \rightleftharpoons S$ pseudorotational equilibria in **1–13** in the neutral form with the kinetic data for the corresponding deglycosylation reaction²⁰ shows that as the anomeric effect increases the stability of the glycosidic bond also increases (relative stabilities in the acid promoted deglycosylation reaction^{1a,20} decrease in the following order: cytidine \approx uridine > guanosine > adenosine). Upon protonation of the nucleobase, the anomeric effect increases more in the ribo series as a result of the contribution from the constituent 2'-OH than in 2'-deoxynucleosides, which is evident from more positive ΔH^{P} values for **8–13** compared to **1–6** (Table 8). Noteworthy also is the fact that the acid-promoted deglycosylation studies²⁰ have shown that ribonucleosides are much more stable than 2'-deoxynucleosides. The strengthening of the anomeric effect in ribonucleosides can be attributed to the effect of 2'-OH group, which inductively decreases the electron density of C1' compared to its 2'-deoxy counterpart.

(4) The extent of the preference of the pentofuranosyl moiety for N pseudorotamers as a function of pD displays a sigmoidal behavior characteristic of a titration curve. Subsequent calculation of the pD values at the inflection points of the titration curves are in accordance with pK_a values of the protonation and deprotonation of the nucleobases available in the literature and those calculated from the pD dependent aromatic and H1' chemical shifts.

(5) Nucleotides and metal ions are involved in the basic metabolic processes of life. There is evidence^{21a} (NMR and UV) that many 3d transition-metal ions (Mn²⁺, Co²⁺,

Ni²⁺, Cu²⁺, Zn²⁺, Cd²⁺) coordinate to both N7 and 5'-phosphate of adenosine and guanosine either directly or via a coordinated water molecule,^{21b} whereas hard metal ions like Mg²⁺ are mainly involved in phosphate binding. It has been known for some time now that the anticancer drug *cis*-Pt(NH₃)₂Cl₂ binds to DNA through the coordination of platinum at N7 of the adenine and guanine moieties.^{21c} *This N7 metalation under neutral conditions is expected to enhance the strength of the anomeric effect as for the simple protonation in the acidic medium, as discussed above, giving a preferential N-type sugar locally at those N7 metal-coordinated purine-rich junctions in DNA.* On the other hand, Hg²⁺ ion binds to the AT-tract of DNA and induces conformational transition from B-DNA to a new conformer.²² The slow titration with HgClO₄ has shown that it binds to N3 of thymine, thereby disrupting the Watson–Crick hydrogen bond of the A–T base pairs and forming a bulge. *Our present study shows that the binding of Hg²⁺ ion to N3 of thymine would be expected to bring about an almost equivalent change in its sugar conformation as we found for the deprotonated thymidine in the alkaline pD, disfavoring the anomeric effect, which consequently is expected to shift the local $N \rightleftharpoons S$ sugar equilibrium to the S-type.*

(6) The pK_a of one particular adenine base close to the cleavage site in ribozyme (leadzyme) has been found to be 6.5,²³ which is unusually high compared to a pK_a of 3.5 for adenosine. Similarly, a study of the pH-dependent equilibrium binding constant revealed that the stability of pyrimidine oligonucleotides with 2'-deoxycytidine and 2'-deoxy-5-methylcytidine to form the local triple-helical structure increases 10- and 20-fold, respectively, as the pH is decreased from 7.6 to 5.8. An analysis of these data has shown that the pK_a of cytosine and 5-methylcytosine bases in triplex DNA goes up to 5.5 [d(C+GC) triplets] and 5.7 [d(m⁵C+GC) triplets] in the above local triple-helical structure compared to pK_a of 4.3 for 2'-deoxycytidine and 4.4 for 5-methyl-2'-deoxycytidine.^{24,25} *This implies that some specific adenine or cytidine nucleotides under certain folded structural states would form the protonated species at a pH close to the physiological pH and, thereby, are more locally vulnerable to take up the preferential N-type conformation, dictating the local change of sugar–phosphate backbone, rather than the other adenine or cytosine residues in the molecule.*

Further work is in progress in our lab to reparametrize the nucleic acid force field for Molecular Mechanic calculations and model-building by employing our present experimental thermodynamic data on the gauche and anomeric effects driven $N \rightleftharpoons S$ equilibrium. Clearly, the work described herein shows that the influence of the specific gauche and anomeric effects exhibited in the drive of the $N \rightleftharpoons S$ equilibrium are characteristic of the exact chemical nature of the nucleobase, which, in turn dictates its chemical response to the composition of the aqueous medium. Further understanding of the impact of various nucleobase-specific gauche and anomeric effects in folded DNA or RNA in a defined aqueous medium should be able to shade light on how the sequence-

(17) (a) Feigon, J.; Wang, A. H. -J.; van der Marel, G. A.; van Boom, J. H.; Rich, A. *Nucl. Acids Res.* **1984**, *12*, 1243. (b) Tran-Dinh, S.; Taboury, J.; Neumann, J. -M.; Huynh-Dinh, T.; Genissel, B.; Laglois d'Estaintot, B.; Igolen, J. *Biochemistry* **1984**, *23*, 1362.

(18) (a) Davis, P. W.; Hall, K.; Cruz, P.; Tinoco, I.; Neilson, T. *Nucl. Acids Res.* **1986**, *14*, 1279. (b) Davis, P. W.; Adamiak, R. W.; Tinoco, I. *Biopolymers* **1990**, *29*, 109.

(19) (a) Agback, P.; Sandstrom, A.; Yamakage, S.-I.; Sund, C.; Glemarec, C.; Chattopadhyaya, J. *J. Biochem. Biophys. Methods* **1993**, *27*, 229. (b) Agback, P.; Glemarec, C.; Yin, L.; Sandstrom, A.; Plavec, J.; Sund, C.; Yamakage, S. -I.; Wiswanadham, G.; Rouse, B.; Puri, N.; Chattopadhyaya, J. *Tetrahedron Lett.* **1993**, *34*, 3929.

(20) Remaud, G.; Zhou, X.-x.; Chattopadhyaya, J.; Oivanan, M.; Lönnberg, H. *Tetrahedron* **1987**, *43*, 4453.

(21) (a) *Metal–DNA Chemistry*; Tullius, T. D., Ed.; ACS Symposium Series; American Chemical Society: Washington, DC, **1989**. (b) Sigel, H. In ref 23a, p 159. (c) Marzilli, L. G.; Kline T. P.; Live, D.; Zon, G. *Ibid.* p 119.

(22) Froeystein, N. Å; Sletten, E. *J. Am. Chem. Soc.* **1994**, *116*, 3240.

(23) Legault, P.; Pardi, A. *J. Am. Chem. Soc.* **1994**, *116*, 8390.

(24) (a) Povsic, T. J.; Dervan, P. B. *J. Am. Chem. Soc.* **1989**, *111*, 3059. (b) Singleton, S. F.; Dervan, P. B. *Biochemistry* **1992**, *31*, 10995. (c) Best, G. C.; Dervan, P. B. *J. Am. Chem. Soc.* **1995**, *117*, 1187.

(25) Xodo, L. E.; Manzini, G.; Quadrifoglio, F.; van der Marel, G. A.; van Boom, J. H. *Nucl. Acids Res.* **1991**, *19*, 5625.

specificity of DNA or RNA dictates the geometry of their local structures and consequently their molecular recognition.

Experimental Section

(A) ¹H-NMR Spectroscopy. ¹H-NMR spectra were recorded at 500 MHz (Bruker AMX 500) in D₂O solution [20 mM for all compounds but 5 mM for dG (**2**) and G (**9**), $\delta_{\text{CH}_3\text{CN}} = 2.00$ ppm as internal reference] between 278 and 358 K at 10 K intervals (also at 5 K intervals for **2**, **5**, and **9**) in the following pD ranges: 1.5–6.1 for **1** (11 pDs, see Table S1 in the supporting information), 1.0–11.4 for **2** (22 pDs, see Table S3 in the supporting information), 1.3–6.4 for **3** (14 pDs, see Table S2 in the supporting information), 7.4–11.6 for **4** (10 pDs, see Table S4 in the supporting information), 7.5–11.9 for **5** (9 pDs, see Table S5 in the supporting information), 4.0–11.8 for FdU **6** (13 pD's, see Table S6 in the supporting information), 2.4–10.8 for **7** (10 pD's, see Table S7 in the supporting information), 1.2–6.5 for **8** (10 pDs, see Table S1 in the supporting information), 0.6–12.0 for **9** (22 pDs, see Table S3 in the supporting information), 1.2–6.6 for **10** (12 pDs, see Table S2 in the supporting information), 5.0–12.0 for **11** (12 pDs, see Table S4 in the supporting information), 7.4–12.0 for **12** (11 pDs, see Table S5 in the supporting information) and 5.1–11.9 for FU (**13**) (12 pDs, see Table S6 in the supporting information). The pD values correspond to the reading on a pH meter equipped with a calomel electrode calibrated with pH 4 and 7 standard buffers in H₂O and are not corrected for the deuterium isotope effect. The pD of the samples has been adjusted by the simple addition of microliter volumes of concentrated D₂SO₄ or NaOD solutions. All spectra have been recorded using 64 K data points and eight scans. The assignments in **1–6** and in **8–13** have been based on ¹H 1D homonuclear decoupling experiments. For **7**, the relative assignments of H_a, H_b, and H_c were obtained from 1D ¹H-NOE difference experiments. The pD-dependent accurate ³J_{HH} (± 0.1 Hz) (Tables 1–7) were obtained through simulation and iteration using DAISY program package¹² and have been used for the pseudorotational analyses.

(B) Conformational Analyses. PSEUROT Fitting Process. The experimental ³J_{HH} coupling constants of **1–13** were translated into rapid two-state equilibrium between a puckered N-type and a puckered S-type furanose ring with the computer program PSEUROT (version 5.4),¹³ which is based on the pseudorotational concept¹⁴ and the generalized Karplus equation.^{13b,c} According to the pseudorotational concept, the conformation of a puckered furanose ring can be described with only two parameters: a phase angle of pseudorotation (P), which defines the part of the ring which is mostly puckered, and a puckering amplitude (Ψ_m), which indicates the extent of puckering.¹⁴ The generalized Karplus equation links coupling constants between vicinal protons to corresponding proton–proton torsion angles. The following λ substituent parameters were used for the substituents on H–C–C–H fragments: $\lambda(\text{C}1') = \lambda(\text{C}3') = \lambda(\text{C}4') = 0.62$; $\lambda(\text{C}2') = 0.67$ in **1–7** and 0.62 in **8–13**; $\lambda(\text{C}5') = 0.68$; $\lambda(\text{O}4') = 1.27$; $\lambda(\text{OH}) = 1.26$ and $\lambda(\text{glycosyl N}) = 0.58$.^{13e,f} We have, however, also found that a change in the value of $\lambda(\text{glycosyl N})$ in the range from 0.3 to 1.2 has a negligible influence on the thermodynamics of the North (N) \rightleftharpoons South (S) equilibrium in the case of both 2'-deoxyribonucleosides and ribonucleosides. The PSEUROT analyses of temperature dependent ³J_{HH} (278–358 K, see Tables S1–S7 in the supporting information) of the sugar moieties of **1–13** at different pDs have been performed in two ways: (i) when there is no bias to the N- or S-type conformations, $\Psi_m(\text{N})$ and $\Psi_m(\text{S})$ have been assumed identical and were kept fixed at identical values during the PSEUROTs, while P_N and P_S were optimized freely. (ii) When one type of conformers is preferred by >65%, the geometry of the minor conformers has been fixed by constraining their P and Ψ_m , while P and Ψ_m of the major conformers were optimized freely. Several PSEUROTs (see below for specific description of the conformational spaces covered by the analyses) were performed for **1–13** at each pD value in order to carefully examine the

conformational hyperspace that is accessible for the N and S conformers of the constituent sugar moieties within a minimal deviation between the experimental and back-calculated coupling constants expressed in terms of both ΔJ_{max} and an rms¹³ (see below). The sets of populations of N and S conformers at several temperatures (see Tables 1–7) at several pDs obtained from the individual corresponding PSEUROT optimizations were used to make the same number of van't Hoff plots. The average slopes and intercepts (see below) of these van't Hoff plots (see Figure 1 and its legend for representative van't Hoff plots) have been subsequently used to calculate ΔH° and ΔS° (and their standard deviations) of the N \rightleftharpoons S sugar equilibrium of **1–13** (Tables 1–7).

dA (**1**). $\Psi_m(\text{N})$ and $\Psi_m(\text{S})$ have been first fixed to identical values from 29° to 36° at 1.5 < pD < 3.8 and from 30° to 37° at 4.1 < pD < 6.1 in 1° steps. At each pD, the phase angles of the N and S conformers optimized during these eight PSEUROTs are $-23^\circ < P_N < 15^\circ$ and $142^\circ < P_S < 159^\circ$. Additionally, at 4.1 < pD < 6.1, P_N of the minor N conformers has been fixed at $-30^\circ \leq P_N \leq 30^\circ$ in 20° steps with $\Psi_m(\text{N})$ being simultaneously fixed at 30°, 33°, and 37° during 12 PSEUROTs which resulted in $141^\circ < P_S < 164^\circ$ and $31^\circ < \Psi_m(\text{S}) < 38^\circ$ ($\Delta J_{\text{max}} < 0.5$ Hz and rms < 0.3 Hz). The eight sets of populations of N and S conformers at nine temperatures (see Table 1 and Table S1 in the supporting information) at seven different pDs below 3.8 and 20 sets at 4 different pDs above 4.1 obtained from the individual corresponding PSEUROT optimizations were used to make the same number of van't Hoff plots. At 1.5 < pD < 3.8, the average slopes and intercepts from eight van't Hoff plots are 0.09–0.28 ($\sigma = 0.01$) and -0.22 to $+0.22$ ($\sigma = 0.02$); at 4.1 < pD < 6.1, the average slopes and intercepts from 20 van't Hoff plots are 0.38–0.46 ($\sigma = 0.01$) and -0.71 to -0.53 ($\sigma = 0.08$). The correlation coefficients (*R*) of the van't Hoff plots are as follows: 0.964 (pD 1.5), 0.985 (pD 2.1), 0.955 (pD 2.6), 0.931 (pD 3.0), 0.966 (pD 3.4), 0.985 (pD 3.6), 0.994 (pD 3.8), 0.997 (pD 4.1), 0.996 (pD 4.5), 0.996 (pD 5.0) and 0.997 (pD 6.1).

dG (**2**). At each pD, $\Psi_m(\text{N})$ and $\Psi_m(\text{S})$ have been first fixed to identical values from 30° to 36° in 1° steps. The phase angles of the N and S conformers optimized during these seven PSEUROTs are $-20^\circ < P_N < 20^\circ$ and $141^\circ < P_S < 158^\circ$. Additionally, at 3.0 < pD < 11.4, P_N of the minor N conformers has been fixed at $-30^\circ \leq P_N \leq 30^\circ$ in 20° steps with $\Psi_m(\text{N})$ being simultaneously fixed at 30°, 33°, and 36° during 12 PSEUROTs which resulted in $139^\circ < P_S < 164^\circ$ and $31^\circ < \Psi_m(\text{S}) < 38^\circ$ ($\Delta J_{\text{max}} < 0.5$ Hz and rms < 0.3 Hz). The seven sets of temperature-dependent populations of N and S conformers at seven different pDs below 2.8 and 19 sets at 15 different pDs above 3.0 obtained from the individual corresponding PSEUROTs were used to make the same number of van't Hoff plots. At 1.0 < pD < 2.8, the average slopes and intercepts from seven van't Hoff plots are -0.22 to $+0.10$ ($\sigma = 0.01$) and 0.23 – 1.06 ($\sigma = 0.02$); at 3.0 < pD < 11.4, the average slopes and intercepts from 19 van't Hoff plots are 0.21–0.60 ($\sigma = 0.01$) and -0.92 to -0.08 ($\sigma = 0.08$). The correlation coefficients (*R*) of the van't Hoff plots are as follows: 0.956 (pD 1.0), 0.958 (pD 1.2), 0.983 (pD 1.5), 0.987 (pD 1.8), 0.960 (pD 2.2), 0.775 (pD 2.5), 0.990 (pD 2.8), 0.971 (pD 3.0), 0.999 (pD 3.2), 0.994 (pD 3.6), 0.996 (pD 4.0), 0.999 (pD 5.0), 0.989 (pD 6.2), 0.996 (pD 7.5), 0.994 (pD 8.4), 0.994 (pD 8.9), 0.996 (pD 9.3), 0.999 (pD 9.7), 0.995 (pD 10.0), 0.997 (pD 10.5), 0.999 (pD 10.9), and 0.999 (pD 11.4). The significance of the Pearson's correlation coefficient at pD 2.5 is limited as the change of the ratio of the molar fractions of N and S pseudorotamers as a function of the inverted temperature (*i.e.*, reflected in the small slopes of the van't Hoff plots) at this pD is negligible and results in ΔH° value of N \rightleftharpoons S equilibria of **2** close to zero (see Table 2).

dC (**3**). At each pD, $\Psi_m(\text{N})$ and $\Psi_m(\text{S})$ have been first fixed to identical values from 29° to 36° in 1° steps. The phase angles of the N and S conformers optimized during these eight PSEUROTs are included in the ranges $-23^\circ < P_N < 4^\circ$ and $132^\circ < P_S < 149^\circ$. ($\Delta J_{\text{max}} = 0.6$ Hz and rms = 0.3 Hz). The eight sets of temperature-dependent populations of N and S conformers at 14 different pDs issued from the individual corresponding PSEUROT optimizations were used to make the same number of van't Hoff plots. At each pD in the range 1.3

$< pD < 6.4$, the average slopes and intercepts from eight van't Hoff plots are -0.01 to $+0.09$ ($\sigma = 0.01$) and 0.19 – 0.34 ($\sigma = 0.02$). The correlation coefficients (R) of the van't Hoff plots are as follows: 0.28 (pD 1.3), 0.54 (pD 1.9), 0.71 (pD 2.2), 0.30 (pD 2.6), 0.17 (pD 3.1), 0.18 (pD 3.6), 0.59 (pD 3.8), 0.80 (pD 4.1), 0.91 (pD 4.3), 0.96 (pD 4.5), 0.97 (pD 4.8), 0.98 (pD 5.2), 0.98 (pD 5.7), and 0.98 (pD 6.4).

dU (4). At each pD, $\Psi_m(N)$ and $\Psi_m(S)$ have been first fixed to identical values from 29° to 35° in 1° steps. The phase angles of the N and S conformers optimized during these seven PSEUROTs are $-15^\circ < P_N < 7^\circ$ and $133^\circ < P_S < 145^\circ$. Additionally, at each pD, P_N of the minor N-type conformers has been fixed at $-30^\circ \leq P_N \leq 30^\circ$ in 20° steps with $\Psi_m(N)$ being simultaneously fixed at 29° , 32° , and 35° during 12 PSEUROTs which resulted in $127^\circ < P_S < 156^\circ$ and $30^\circ < \Psi_m(S) < 39^\circ$ ($\Delta J_{\max} = 0.5$ Hz and rms = 0.3 Hz). The 19 sets of temperature-dependent populations of N and S conformers at 10 different pDs from 7.4 to 11.6 issued from the individual corresponding PSEUROTs were used to make the same number of van't Hoff plots. At each pD, the average slopes and intercepts from 19 van't Hoff plots are 0.07 – 0.16 ($\sigma = 0.01$) and 0.04 – 0.20 ($\sigma = 0.10$). The correlation coefficients (R) of the van't Hoff plots are as follows: 0.933 (pD 7.4), 0.916 (pD 8.1), 0.921 (pD 8.6), 0.965 (pD 9.0), 0.964 (pD 9.4), 0.932 (pD 9.8), 0.984 (pD 10.2), 0.978 (pD 10.7), 0.983 (pD 11.1), and 0.986 (pD 11.6).

T (5). At each pD, $\Psi_m(N)$ and $\Psi_m(S)$ have been first fixed to identical values from 29° to 36° in 1° steps. The phase angles of the N and S conformers optimized during these eight PSEUROTs are $-24^\circ < P_N < 31^\circ$ and $126^\circ < P_S < 147^\circ$ ($\Delta J_{\max} = 0.6$ Hz and rms = 0.3 Hz). The eight sets of temperature-dependent populations of N and S conformers at nine different pDs from 7.5 to 11.9 obtained from the individual PSEUROTs were used to make the same number of van't Hoff plots. At each pD, the average slopes and intercepts from eight van't Hoff plots are 0.16 – 0.25 ($\sigma = 0.01$) and -0.18 to 0.00 ($\sigma = 0.05$). The correlation coefficients (R) of the van't Hoff plots are as follows: 0.957 (pD 7.5), 0.907 (pD 8.3), 0.870 (pD 8.9), 0.975 (pD 9.3), 0.973 (pD 9.7), 0.963 (pD 10.0), 0.958 (pD 10.4), 0.979 (pD 11.2), and 0.930 (pD 11.9).

FdU (6). At each pD, $\Psi_m(N)$ and $\Psi_m(S)$ have been first fixed to identical values from 29° to 36° in 1° steps. The phase angles of the N and S conformers optimized during these eight PSEUROTs are $-24^\circ < P_N < 5^\circ$ and $130^\circ < P_S < 147^\circ$ ($\Delta J_{\max} = 0.5$ Hz and rms = 0.3 Hz). The eight sets of temperature-dependent populations of N and S conformers at 13 different pDs from 4.0 to 11.8 issued from the individual corresponding PSEUROTs were used to make the same number of van't Hoff plots. At each pD in the range $4.0 < pD < 11.8$, the average slopes and intercepts from eight van't Hoff plots are 0.08 – 0.14 ($\sigma = 0.01$) and 0.09 – 0.20 ($\sigma = 0.03$). The correlation coefficients (R) of the van't Hoff plots areas follows: 0.987 (pD 4.0), 0.929 (pD 6.1), 0.913 (pD 6.6), 0.950 (pD 7.0), 0.885 (pD 7.4), 0.924 (pD 7.9), 0.948 (pD 8.2), 0.980 (pD 8.5), 0.967 (pD 9.0), 0.985 (pD 9.5), 0.979 (pD 10.1), 0.968 (pD 10.7), and 0.986 (pD 11.8).

dImb (7). At each pD, $\Psi_m(N)$ and $\Psi_m(S)$ have been first fixed to identical values from 30° to 36° at pD 3.3 and 5.0, from 30° to 37° at pD 2.4, 5.4, 6.4, and $6.9 < pD < 10.8$, from 31° to 36° at pD 6.9, and from 31° to 37° at pD 6.0 in 1° steps. The phase angles of the N and S conformers optimized during these PSEUROTs are included in the ranges $-25^\circ < P_N < 0^\circ$ and $135^\circ < P_S < 154^\circ$. ($\Delta J_{\max} = 0.5$ Hz and rms = 0.3 Hz). The six sets of temperature-dependent populations of N and S conformers at pD 6.9, seven sets at pD 3.3, 5.0, and 6.0, and eight sets at pD 2.4, 5.4, 6.4, and $6.9 < pD < 10.8$ issued from the individual corresponding PSEUROTs were used to make the same number of van't Hoff plots. At pD 6.9, the average slopes and intercepts from the six van't Hoff plots are 0.21 ($\sigma = 0.01$) and -0.20 ($\sigma = 0.01$). At pD 3.3, 5.0, and 6.0, the average slopes and intercepts from the seven van't Hoff plots are from -0.01 to $+0.09$ ($\sigma = 0.01$) and from -0.03 to $+0.12$ ($\sigma = 0.01$). At pD 2.4, 5.4, 6.4, and $6.9 < pD < 10.8$, the average slopes and intercepts from the eight van't Hoff plots are -0.02 to $+0.29$ ($\sigma = 0.01$) and -0.42 to $+0.12$ ($\sigma = 0.02$). The correlation coefficients (R) of the van't Hoff plots are as

follows: 0.746 (pD 2.4), 0.129 (pD 3.3), 0.229 (pD 5.0), 0.398 (pD 5.4), 0.777 (pD 6.0), 0.912 (pD 6.4), 0.979 (pD 6.9), 0.991 (pD 7.9), 0.988 (pD 9.7), and 0.977 (pD 10.8). Note that the significance of the Pearson's correlation coefficients below pD 6.0 is limited as the change of the ratio of the molar fractions of N and S pseudorotamers as a function of the inverted temperature (*i.e.*, reflected in the small slopes of the van't Hoff plots) at these pDs is negligible and results in ΔH° values of $N \rightleftharpoons S$ equilibria of **7** close to zero (see Table 7).

A (8). At each pD, $\Psi_m(N)$ and $\Psi_m(S)$ have been first fixed to identical values from 29° to 39° in 1° steps. The phase angles of the N and S conformers optimized during these 11 PSEUROTs are included in the ranges $-35^\circ < P_N < 43^\circ$ and $128^\circ < P_S < 170^\circ$ ($\Delta J_{\max} = 0.4$ Hz and rms = 0.2 Hz). The 11 sets of temperature-dependent populations of N and S conformers at 10 pDs from 1.2 to 6.5 issued from the individual corresponding PSEUROTs were used to make the same number of van't Hoff plots. At each pD from 1.2 to 6.5, the average slopes and intercepts from the 11 van't Hoff plots are 0.03 to 0.51 ($\sigma = 0.01$) and -1.01 to $+0.17$ ($\sigma = 0.01$). The correlation coefficients (R) for the linear relationship of the 11 van't Hoff plots at each pD are as follows: 0.750 (pD 1.2), 0.806 (pD 1.9), 0.669 (pD 2.4), 0.910 (pD 2.9), 0.991 (pD 3.4), 0.994 (pD 3.7), 0.994 (pD 4.3), 0.995 (pD 5.0), 0.992 (pD 5.7), and 0.995 (pD 6.5). The significance of the Pearson's correlation coefficients below pD 2.9 is limited as the change of the ratio of the molar fractions of N and S pseudorotamers as a function of the inverted temperature (*i.e.*, reflected in the small slopes of the van't Hoff plots) at these pDs is negligible and results in ΔH° values of $N \rightleftharpoons S$ equilibria of **8** close to zero (see Table 1).

G (9). $\Psi_m(N)$ and $\Psi_m(S)$ have been first fixed to identical values in the range from 30° to 37° at $0.6 < pD < 7.5$ and from 30° to 38° at $8.5 < pD < 12.0$ in 1° steps. The phase angles of the N and S conformers optimized during these eight (below pD 7.5) or nine (above pD 8.5) PSEUROTs are $-36^\circ < P_N < 45^\circ$ and $127^\circ < P_S < 170^\circ$. Additionally, at pD 0.6, 0.9, P_S of the minor S-type conformers has been fixed at $150^\circ \leq P_S \leq 180^\circ$ in 10° steps with $\Psi_m(S)$ being simultaneously fixed at 30° , 33° , and 37° during 12 PSEUROTs which resulted in $10^\circ < P_N < 29^\circ$ and $30^\circ < \Psi_m(N) < 37^\circ$, whereas at each pD in the range $3.6 < pD < 12.0$, P_N of the minor N-type conformers has been fixed at $-30^\circ \leq P_N \leq 30^\circ$ in 20° steps with $\Psi_m(N)$ being simultaneously fixed at 30° , 34° and 38° during 12 PSEUROT optimizations which resulted in $130^\circ < P_S < 162^\circ$ and $28^\circ < \Psi_m(S) < 45^\circ$ ($\Delta J_{\max} = 0.4$ Hz and rms = 0.2 Hz). The several sets of temperature-dependent populations of N and S conformers (20 sets at pD 0.6 and 0.9, eight sets at $1.2 < pD < 3.0$, 20 at $3.6 < pD < 7.5$, and 21 at $8.5 < pD < 12.0$) obtained from the individual corresponding PSEUROT optimizations were used to make the same number of van't Hoff plots. At pD 0.6 and 0.9, the average slopes and intercepts from the 20 van't Hoff plots are -0.59 to -0.55 ($\sigma = 0.02$) and 1.32 – 1.42 ($\sigma = 0.10$). At each pD in the range $1.2 < pD < 3.0$, the average slopes and intercepts from the eight van't Hoff plots are -0.62 to $+0.28$ ($\sigma = 0.02$) and -0.43 to $+1.85$ ($\sigma = 0.03$). At each pD in the range $3.6 < pD < 7.5$, the average slopes and intercepts from the 20 van't Hoff plots are 0.39 – 0.41 ($\sigma = 0.02$) and -0.76 to -0.72 ($\sigma = 0.09$). At each pD in the range $8.5 < pD < 12.0$, the average slopes and intercepts from the 21 van't Hoff plots are 0.48 – 0.93 ($\sigma = 0.06$) and -1.99 to -0.94 ($\sigma = 0.07$). The correlation coefficients (R) of the van't Hoff plots are as follows: 0.994 (pD 0.6), 0.977 (pD 0.9), 0.994 (pD 1.2), 0.987 (pD 1.5), 0.976 (pD 1.8), 0.976 (pD 1.9), 0.974 (pD 2.3), 0.544 (pD 2.7), 0.989 (pD 3.0), 0.988 (pD 3.6), 0.996 (pD 4.4), 0.997 (pD 6.4), 0.989 (pD 7.5), 0.992 (pD 8.5), 0.996 (pD 9.1), 0.996 (pD 9.4), 0.995 (pD 9.7), 0.998 (pD 10.0), 0.998 (pD 10.4), 0.999 (pD 10.9), 0.996 (pD 11.5), and 0.998 (pD 12.0). Note that the significance of the Pearson's correlation coefficients at pD 2.7 is limited as the change of the ratio of the molar fractions of N and S pseudorotamers as a function of the inverted temperature (*i.e.*, reflected in the small slopes of the van't Hoff plots) at this pD is negligible and results in ΔH° value of $N \rightleftharpoons S$ equilibria of **9** close to zero (see Table 2).

C (10). $\Psi_m(N)$ and $\Psi_m(S)$ have been first fixed to identical values in the range from 30° to 38° at $1.2 < pD < 4.2$, from

30° to 37° at pD 4.7 and 5.3, and from 30° to 36° at pD 5.8 and 6.6. The phase angles of the N and S conformers optimized during these nine (at 1.2 < pD < 4.2), eight (at pD 4.7 and 5.3), or seven (at pD 5.8 and 6.6) PSEUROTs are $-19^\circ < P_N < 31^\circ$ and $113^\circ < P_S < 153^\circ$. Additionally, P_S of the minor S-type conformers has been fixed at $150^\circ \leq P_S \leq 180^\circ$ in 10° steps with Ψ_m (S) being simultaneously fixed at 30°, 34°, and 38° at 1.2 < pD < 4.2, 30°, 34°, and 37° at pD 4.7 and 5.3, at 30°, 33°, and 36° at pD 5.8, and 6.6 during 12 PSEUROTs which resulted in $24^\circ < P_N < 44^\circ$ and $30^\circ < \Psi_m$ (N) < 38° ($\Delta J_{\max} < 0.5$ Hz and rms < 0.3 Hz). The several sets of temperature-dependent populations of N and S conformers (21 sets at 1.2 < pD < 4.2, 20 sets at pD 4.7 and 5.3, 19 at pD 5.8 and 6.6) obtained from the individual corresponding PSEUROTs were used to make the same number of van't Hoff plots. At 1.2 < pD < 4.2, the average slopes and intercepts from the 21 van't Hoff plots are -0.62 to -0.43 ($\sigma = 0.03$) and 0.78 to 1.34 ($\sigma = 0.17$). At pD 4.7 and 5.3, the average slopes and intercepts from the 20 van't Hoff plots are -0.34 to $+0.30$ ($\sigma = 0.02$) and 0.39 – 0.52 ($\sigma = 0.22$). At pD 5.8 and 6.6, the average slopes and intercepts from the 19 van't Hoff plots are -0.30 to -0.27 ($\sigma = 0.01$) and 0.33 – 0.43 ($\sigma = 0.18$). The correlation coefficients (R) of the van't Hoff plots are as follows: 0.988 (pD 1.2), 0.994 (pD 1.8), 0.987 (pD 2.3), 0.992 (pD 2.8), 0.980 (pD 3.3), 0.986 (pD 3.7), 0.990 (pD 4.0), 0.993 (pD 4.2), 0.996 (pD 4.7), 0.990 (pD 5.3), 0.990 (pD 5.8), and 0.999 (pD 6.6).

U (11): Ψ_m (N) and Ψ_m (S) have been first fixed to identical values from 29° to 36° at each pD in the range 5.0 < pD < 12.0. The phase angles of the N and S conformers optimized during these eight PSEUROTs are $-19^\circ < P_N < +32^\circ$ and $116^\circ < P_S < 143^\circ$ ($\Delta J_{\max} < 0.4$ Hz and rms < 0.2 Hz). The eight sets of temperature-dependent populations of N and S conformers at each pD obtained from the individual corresponding PSEUROTs were used to make the same number of van't Hoff plots. The average slopes and intercepts from the 8 van't Hoff plots at each pD are -0.26 to -0.02 ($\sigma = 0.01$) and 0.05 – 0.73 ($\sigma = 0.12$). The correlation coefficients (R) of the van't Hoff plots are as follows: 0.975 (pD 5.0), 0.966 (pD 7.3), 0.954 (pD 7.9), 0.992 (pD 8.4), 0.965 (pD 8.9), 0.963 (pD 9.3), 0.944 (pD 9.7), 0.897 (pD 10.1), 0.882 (pD 10.6), 0.885 (pD 11.1), 0.903 (pD 11.5), and 0.715 (pD 12.0). Note that the significance of the Pearson's correlation coefficients above pD 10.1 is limited as the change of the ratio of the molar fractions of N and S pseudorotamers as a function of the inverted temperature (*i.e.*, reflected in the small slopes of the van't Hoff plots) at these pDs is negligible and results in ΔH° values of N \rightleftharpoons S equilibria of **11** close to zero (see Table 4).

rT (12): Ψ_m (N) and Ψ_m (S) have been first fixed to identical values in the range from 29° to 36° at each pD in the range 7.4 < pD < 12.0. The phase angles of the N and S conformers optimized during these 8 PSEUROTs are $-22^\circ < P_N < 34^\circ$ and $116^\circ < P_S < 141^\circ$ ($\Delta J_{\max} < 0.4$ Hz and rms < 0.2 Hz). The eight sets of temperature-dependent populations of N and S conformers at each pD obtained from the individual corresponding PSEUROTs were used to make the same number of van't Hoff plots. The average slopes and intercepts from the eight van't Hoff plots at each pD are -0.15 to 0.03 ($\sigma = 0.01$) and 0.05 to 0.55 ($\sigma = 0.11$). The correlation coefficients (R) of the van't Hoff plots are as follows: 0.931 (pD 7.4), 0.929 (pD 8.0), 0.853 (pD 8.5), 0.948 (pD 9.0), 0.837 (pD 9.5), 0.690 (pD 9.8), 0.912 (pD 10.1), 0.858 (pD 10.5), 0.283 (pD 11.0), 0.279 (pD 11.4), and 0.710 (pD 12.0). Note that the significance of the Pearson's correlation coefficients above pD 9.0 is limited as the change of the ratio of the molar fractions of N and S pseudorotamers as a function of the inverted temperature (*i.e.*, reflected in the small slopes of the van't Hoff plots) at these pDs is negligible and results in ΔH° values of N \rightleftharpoons S equilibria of **12** close to zero (see Table 5).

FU (13): Ψ_m (N) and Ψ_m (S) have been first fixed to identical values in the range from 30° to 37° at each pD in the range 5.1 < pD < 7.1, from 30° to 36° at pD 7.6 and 8.0, from 29° to 35° at pD 8.5, and from 30° to 35° at 9.0 < pD < 11.9. The phase angles of the N and S conformers optimized during these eight (at 5.1 < pD < 7.1), seven (at pD 7.6, 8.0 and 8.5), or six PSEUROTs (at 9.0 < pD < 11.9) are $-20^\circ < P_N < 30^\circ$ and

$118^\circ < P_S < 146^\circ$ ($\Delta J_{\max} < 0.4$ Hz and rms < 0.2 Hz). The several sets of temperature-dependent populations of N and S conformers (eight at 5.1 < pD < 7.1; seven at pD 7.6, 8.0, and 8.5; 6 at 9.0 < pD < 11.9) obtained from the individual corresponding PSEUROTs were used to make the same number of van't Hoff plots. The average slopes and intercepts from the eight van't Hoff plots at 5.1 < pD < 7.1 are -0.28 to -0.22 ($\sigma = 0.01$) and 0.58 – 0.74 ($\sigma = 0.09$). The average slopes and intercepts from the seven van't Hoff plots at pD 7.6, 8.0, and 8.5 are -0.22 to -0.11 ($\sigma = 0.01$) and 0.25 – 0.60 ($\sigma = 0.11$). The average slopes and intercepts from the six van't Hoff plots at 9.0 < pD < 11.9 are -0.12 to -0.07 ($\sigma = 0.01$) and 0.16 – 0.30 ($\sigma = 0.12$). The correlation coefficients (R) of the van't Hoff plots are as follows: 0.971 (pD 5.1), 0.958 (pD 6.5), 0.963 (pD 7.1), 0.978 (pD 7.6), 0.964 (pD 8.0), 0.951 (pD 8.5), 0.954 (pD 9.0), 0.951 (pD 9.5), 0.843 (pD 10.0), 0.925 (pD 10.4), 0.927 (pD 10.8), and 0.900 (pD 11.9).

(C) Determination of the pK_a Values of the Aglycon from the Hill Plots. The Hill plot for the δH_8 of dA (**1**) where the total change ($\Delta \delta H_{8, \text{tot}}$) of the chemical shift of H8 between the neutral (δ 8.212) and the protonated state (δ 8.473 ppm) of 0.261 ppm is used to calculate the straight line ($R = 0.996$) which is characterized with the slope of 0.91 ($\sigma = 0.04$) and pK_a of 3.62 ($\sigma = 0.02$) (see panel A in Figure S1 in the supporting information). The additional Hill plots (not shown) made for the δH_2 and $\delta H_1'$ of dA (**1**) resulted in an identical value for the pK_a of its adenine base [for H2: δ 8.396 ppm in the protonated state, δ 8.108 ppm in the neutral state; slope = 0.91 ($\sigma = 0.04$), $pK_a = 3.62$ ($\sigma = 0.02$), $R = 0.996$; for H1': δ 6.475 ppm in the protonated state, δ 6.375 ppm in the neutral state; slope = 0.90 ($\sigma = 0.04$), $pK_a = 3.61$ ($\sigma = 0.02$), $R = 0.996$]. The Hill plot for ΔG° of dA (**1**) where the total change between the neutral and the protonated state ($\Delta G^\circ_{\text{tot}}$) of 1.0 kJ/mol is used to calculate the straight line ($R = 0.988$) with the slope of 1.02 ($\sigma = 0.08$) and pK_a of 3.50 ($\sigma = 0.04$) (see panel B) in Figure S1 in the supporting information).

The Hill plot for the δH_8 of dG (**2**) in the acidic solution where the total change of the chemical shift of H8 ($\Delta \delta H_{8, \text{tot}}$) between the neutral (7.919 ppm) and the protonated (9.101 ppm) state of 1.182 ppm is used to calculate the straight line ($R = 0.993$) which is characterized with the slope of 0.87 ($\sigma = 0.05$) and pK_a of 2.24 ($\sigma = 0.03$) (see panel C in Figure S1 in the supporting information). The additional Hill plot (not shown) made for the $\delta H_1'$ of dG (**2**) also resulted in an identical value for the pK_a of its guanine base [δ 6.377 ppm in the protonated state, δ 6.236 ppm in the neutral state; slope = 0.90 ($\sigma = 0.06$), $pK_a = 2.20$ ($\sigma = 0.04$), $R = 0.990$]. The Hill plot for the δH_8 of dG (**2**) in the alkaline solution where the total change of the chemical shift of H8 ($\Delta \delta H_{8, \text{tot}}$) between the neutral (7.919 ppm) and the deprotonated (7.786 ppm) state of 0.133 ppm is used to calculate the straight line ($R = 0.996$) which is characterized with the slope of 0.99 ($\sigma = 0.05$) and pK_a of 9.45 ($\sigma = 0.03$). Note that $\delta H_1'$ of dG (**2**) shows no variation with pD in the alkaline solution and can therefore not be used for the determination of pK_a (see Panel D in Figure S1 in the supporting information). The Hill plot for ΔG° of dG (**2**) where the total change between the neutral and the protonated state ($\Delta G^\circ_{\text{tot}}$) of 1.7 kJ/mol is used to calculate the straight line ($R = 0.984$) with the slope of 0.84 ($\sigma = 0.07$) and pK_a of 2.25 ($\sigma = 0.06$) (see panel E in Figure S1 in the supporting information). The Hill plot for ΔG° of dG (**2**) where the total change between the neutral and the deprotonated state ($\Delta G^\circ_{\text{tot}}$) of 1.0 kJ/mol is used to calculate the straight line ($R = 0.995$) with the slope of 1.13 ($\sigma = 0.06$) and pK_a of 9.47 ($\sigma = 0.03$) (see panel F in Figure S1 in the supporting information).

The Hill plot for the δH_6 of dC (**3**) where the total change ($\Delta \delta H_{6, \text{tot}}$) between the neutral (δ 7.758 ppm) and the protonated (δ 8.036 ppm) state of 0.278 ppm is used to calculate the straight line ($R = 0.998$) which is characterized with the slope of 0.91 ($\sigma = 0.03$) and pK_a of 4.25 ($\sigma = 0.02$) (see panel G in Figure S1 in the supporting information). The additional Hill plots (not shown) made for the δH_5 and $\delta H_1'$ of dC (**3**) also resulted in an identical value for the pK_a of its cytosine base [for H5: δ 6.168 ppm in the protonated state, δ 5.981 ppm in the neutral state; slope = 0.91 ($\sigma = 0.02$), $pK_a = 4.24$

($\sigma = 0.01$), $R = 0.998$; for H1': δ 6.176 ppm in the protonated state, δ 6.200 ppm in the neutral state; slope = 0.95 ($\sigma = 0.06$), $pK_a = 4.21$ ($\sigma = 0.03$), $R = 0.991$]. The Hill plot for ΔG° of dC (**3**) where the total change between the neutral and the protonated state ($\Delta G^\circ_{\text{tot}}$) of 0.5 kJ/mol is used to calculate the straight line ($R = 0.901$) with the slope of 0.9 ($\sigma = 0.1$) and pK_a of 4.2 ($\sigma = 0.2$) (see panel H in Figure S1 in the supporting information).

The Hill plot for the $\delta H6$ of dU (**4**) where the total change ($\Delta\delta H6_{\text{tot}}$) between the neutral (δ 7.776 ppm) and the deprotonated state (δ 7.615 ppm) of 0.161 ppm is used to calculate the straight line ($R = 0.999$) which is characterized with the slope of 0.92 ($\sigma = 0.02$) and pK_a of 9.44 ($\sigma = 0.01$) (see panel I in Figure S1 in the supporting information). The additional Hill plots (not shown) made for the $\delta H5$ and $\delta H1'$ of dU (**4**) also resulted in an identical value for the pK_a of its uracil base [for H5: δ 5.819 ppm in the neutral state, δ 5.742 ppm in the deprotonated state; slope = 0.97 ($\sigma = 0.02$), $pK_a = 9.44$ ($\sigma = 0.01$), $R = 0.999$; for H1': δ 6.212 ppm in the neutral state, δ 6.245 ppm in the deprotonated state; slope = 0.93 ($\sigma = 0.02$), $pK_a = 9.43$ ($\sigma = 0.02$), $R = 0.999$]. The Hill plot for ΔG° of dU (**4**) where the total change between the neutral and the deprotonated state ($\Delta G^\circ_{\text{tot}}$) of 0.36 kJ/mol is used to calculate the straight line ($R = 0.944$) with the slope of 0.6 ($\sigma = 0.1$) and pK_a of 9.5 ($\sigma = 0.1$) (see panel J in Figure S1 in the supporting information).

The Hill plot for the $\delta H6$ of T (**5**) where the total change ($\Delta\delta H6_{\text{tot}}$) between the neutral (δ 7.422 ppm) and the deprotonated state (δ 7.577 ppm) of 0.155 ppm is used to calculate the straight line ($R = 0.997$) which is characterized with the slope of 0.99 ($\sigma = 0.04$) and pK_a of 9.84 ($\sigma = 0.02$) (see panel K in Figure S1 in the supporting information). An additional Hill plot (not shown) made for the $\delta H1'$ of T (**5**) also resulted in an identical value for the pK_a of its thymine base [for H1': δ 6.227 ppm in the neutral state, δ 6.265 ppm in the deprotonated state; slope = 0.87 ($\sigma = 0.04$), $pK_a = 9.84$ ($\sigma = 0.04$), $R = 0.998$]. The Hill plot for ΔG° of T (**5**) where the total change between the neutral and the deprotonated state ($\Delta G^\circ_{\text{tot}}$) of 0.22 kJ/mol is used to calculate the straight line ($R = 0.999$) with the slope of 1.79 ($\sigma = 0.05$) and pK_a of 9.74 ($\sigma = 0.01$) (see panel L in Figure S1 in the supporting information).

The Hill plot for the $\delta H6$ of FdU (**6**) where the total change ($\Delta\delta H6_{\text{tot}}$) between the neutral (δ 7.974 ppm) and the deprotonated state (δ 7.709 ppm) of 0.265 ppm is used to calculate the straight line ($R = 0.999$) which is characterized with the slope of 0.99 ($\sigma = 0.02$) and pK_a of 7.73 ($\sigma = 0.02$) (see panel M in Figure S1 in the supporting information). An additional Hill plot (not shown) made for the $\delta H1'$ of FdU (**6**) also resulted in an identical value for the pK_a of its 5-fluorouracil base [for H1': δ 6.207 ppm in the neutral state, δ 6.218 ppm in the deprotonated state; slope = 1.01 ($\sigma = 0.11$), $pK_a = 7.83$ ($\sigma = 0.08$), $R = 0.973$]. The Hill plot for ΔG° of FdU (**6**) where the total change between the neutral and the deprotonated state ($\Delta G^\circ_{\text{tot}}$) of 0.30 kJ/mol is used to calculate the straight line ($R = 0.978$) with the slope of 0.86 ($\sigma = 0.09$) and pK_a of 7.78 ($\sigma = 0.07$) (see Panel (N) in Figure S1 in the supporting information).

The Hill plot for the δH_a of dImb (**7**) where the total change ($\Delta\delta H_a_{\text{tot}}$) between the neutral (δ 7.461 ppm) and the protonated state (δ 7.002 ppm) of 0.459 ppm is used to calculate the straight line ($R = 0.999$) which is characterized with the slope of 0.98 ($\sigma = 0.02$) and pK_a of 6.02 ($\sigma = 0.01$) (see panel O in Figure S1 in the supporting information). The additional Hill plots (not shown) made for the δH_b and δH_c of dImb (**7**) also resulted in an identical value for the pK_a of its 1-imidazole moiety [for Hb: δ 7.614 ppm in the neutral state, δ 7.265 ppm in the deprotonated state; slope = 0.94 ($\sigma = 0.01$), $pK_a = 6.05$ ($\sigma = 0.01$), $R = 0.999$; for Hc: δ 8.890 ppm in the neutral state, δ 7.819 ppm in the deprotonated state; slope = 0.96 ($\sigma = 0.02$), $pK_a = 6.05$ ($\sigma = 0.01$), $R = 0.999$]. The Hill plot for ΔG° of dImb (**7**) where the total change between the neutral and the deprotonated state ($\Delta G^\circ_{\text{tot}}$) of 1.23 kJ/mol is used to calculate the straight line ($R = 0.999$) with the slope of 1.00 ($\sigma = 0.03$) and pK_a of 6.00 ($\sigma = 0.02$) (see panel P in Figure S1 in the supporting information).

The Hill plot for the $\delta H8$ of A (**8**) where the total change

($\Delta\delta H8_{\text{tot}}$) between the neutral (δ 8.234 ppm) and the protonated state (δ 8.501 ppm) of 0.267 ppm is used to calculate the straight line ($R = 0.998$) which is characterized with the slope of 0.90 ($\sigma = 0.03$) and pK_a of 3.47 ($\sigma = 0.03$) (see panel R in Figure S1 in the supporting information). The additional Hill plots (not shown) made for the $\delta H2$ and $\delta H1'$ of A (**8**) also resulted in an identical value for the pK_a of its adenine base [for H2: δ 8.400 ppm in the protonated state, δ 8.120 ppm in the neutral state; slope = 0.91 ($\sigma = 0.03$), $pK_a = 3.58$ ($\sigma = 0.02$), $R = 0.998$; for H1': δ 6.102 ppm in the protonated state, δ 5.977 ppm in the neutral state; slope = 0.93 ($\sigma = 0.03$), $pK_a = 3.54$ ($\sigma = 0.03$), $R = 0.998$]. The Hill plot for ΔG° of A (**8**) where the total change between the neutral and the protonated state ($\Delta G^\circ_{\text{tot}}$) of 1.3 kJ/mol is used to calculate the straight line ($R = 0.982$) with the slope of 0.74 ($\sigma = 0.08$) and pK_a of 3.49 ($\sigma = 0.07$) (see panel S in Figure S1 in the supporting information).

The Hill plot for the $\delta H8$ of G (**9**) in the acidic solution where the total change ($\Delta\delta H8_{\text{tot}}$) between the neutral (δ 7.926 ppm) and the protonated state (δ 9.113 ppm) of 1.187 ppm is used to calculate the straight line ($R = 0.996$) which is characterized with the slope of 0.94 ($\sigma = 0.03$) and pK_a of 2.12 ($\sigma = 0.03$) (see panel T in Figure S1 in the supporting information). An additional Hill plot (not shown) made for the $\delta H1'$ of G (**9**) also resulted in an identical value for the pK_a of its guanine base [for H1': δ 6.019 ppm in the protonated state, δ 5.840 ppm in the neutral state; slope = 0.98 ($\sigma = 0.05$), $pK_a = 2.15$ ($\sigma = 0.04$), $R = 0.993$]. The Hill plot for the $\delta H8$ of G (**9**) in the alkaline solution ($\Delta\delta H8_{\text{tot}} = 0.147$ ppm; $\delta H8$ neutral state = 7.926 ppm; $\delta H8$ deprotonated state = 7.779 ppm) showing the straight line ($R = 0.998$) with the slope of 0.97 ($\sigma = 0.03$) and pK_a of 9.43 ($\sigma = 0.02$) (see panel U in Figure S1 in the supporting information). An additional Hill plot (not shown) made for the $\delta H1'$ of G (**9**) also resulted in an identical value for the pK_a of its guanine base [for H1': δ 5.840 ppm in the neutral state, δ 5.798 ppm in the deprotonated state; slope = 1.3 ($\sigma = 0.1$), $pK_a = 9.79$ ($\sigma = 0.04$), $R = 0.990$]. The Hill plot for ΔG° of G (**9**) where the total change between the neutral and the protonated state ($\Delta G^\circ_{\text{tot}}$) of 3.0 kJ/mol is used to calculate the straight line ($R = 0.997$) with the slope of 0.96 ($\sigma = 0.04$) and pK_a of 2.12 ($\sigma = 0.02$) (see panel V in Figure S1 in the supporting information). The Hill plot for ΔG° of G (**9**) where the total change between the neutral and the deprotonated state ($\Delta G^\circ_{\text{tot}}$) of 1.3 kJ/mol is used to calculate the straight line ($R = 0.992$) with the slope of 1.10 ($\sigma = 0.07$) and pK_a of 9.59 ($\sigma = 0.04$) (see panel Z in Figure S1 in the supporting information).

The Hill plot for the $\delta H6$ of C (**10**) where the total change ($\Delta\delta H6_{\text{tot}}$) between the neutral (δ 8.079 ppm) and the protonated (δ 7.768 ppm) state of 0.311 ppm is used to calculate the straight line ($R = 0.996$) which is characterized with the slope of 0.98 ($\sigma = 0.04$) and pK_a of 4.13 ($\sigma = 0.03$) (see panel a in Figure S1 in the supporting information). An additional Hill plot (not shown) made for the $\delta H5$ of C (**10**) also resulted in an identical value for the pK_a of its cytosine base [for H5: δ 6.180 ppm in the protonated state, δ 5.981 ppm in the neutral state; slope = 0.95 ($\sigma = 0.05$), $pK_a = 4.10$ ($\sigma = 0.04$), $R = 0.994$]. The Hill plot for ΔG° of C (**10**) where the total change between the neutral and the protonated state ($\Delta G^\circ_{\text{tot}}$) of 0.4 kJ/mol is used to calculate the straight line ($R = 0.935$) with the slope of 1.2 ($\sigma = 0.2$) and pK_a of 4.0 ($\sigma = 0.1$) (see panel b in Figure S1 in the supporting information).

The Hill plot for the $\delta H6$ of U (**11**) where the total change ($\Delta\delta H6_{\text{tot}}$) between the neutral (δ 7.607 ppm) and the deprotonated (δ 7.802 ppm) state of 0.195 ppm is used to calculate the straight line ($R = 0.997$) which is characterized with the slope of 1.01 ($\sigma = 0.05$) and pK_a of 9.38 ($\sigma = 0.03$) (see panel c in Figure S1 in the supporting information). An additional Hill plot (not shown) made for the $\delta H5$ of U (**11**) also resulted in an identical value for the pK_a of its uracil base [for H5: δ 5.829 ppm in the neutral state, δ 5.740 ppm in the deprotonated state; slope = 0.97 ($\sigma = 0.05$), $pK_a = 9.34$ ($\sigma = 0.03$), $R = 0.996$]. The Hill plot for ΔG° of U (**11**) where the total change between the neutral and the deprotonated state ($\Delta G^\circ_{\text{tot}}$) of 0.2 kJ/mol is used to calculate the straight line ($R = 0.906$)

with the slope of 1.3 ($\sigma = 0.3$) and pK_a of 9.6 ($\sigma = 0.15$) (see panel d in Figure S1 in the supporting information).

The Hill plot for the δH_6 of rT (**12**) where the total change ($\Delta\delta H_{6_{tot}}$) between the neutral (δ 7.618 ppm) and the deprotonated (δ 7.427 ppm) state of 0.191 ppm is used to calculate the straight line ($R = 0.997$) which is characterized with the slope of 0.98 ($\sigma = 0.05$) and pK_a of 9.76 ($\sigma = 0.02$) (see panel e in Figure S1 in the supporting information). An additional Hill plot (not shown) made for the $\delta H_{1'}$ of rT (**12**) also resulted in an identical value for the pK_a of its thymine base [For $H_{1'}$: δ 5.850 ppm in the neutral state, δ 5.766 ppm in the deprotonated state; slope = 0.84 ($\sigma = 0.08$), $pK_a = 9.60$ ($\sigma = 0.04$), $R = 0.990$]. The Hill plot for ΔG° of rT (**12**) where the total change between the neutral and the deprotonated state (ΔG°_{tot}) of 0.2 kJ/mol is used to calculate the straight line ($R = 0.965$) with the slope of 0.9 ($\sigma = 0.1$) and pK_a of 9.86 ($\sigma = 0.08$) (see panel f in Figure S1 in the supporting information).

The Hill plot for the δH_6 of FU (**13**) where the total change ($\Delta\delta H_{6_{tot}}$) between the neutral (δ 8.039 ppm) and the protonated (δ 7.733 ppm) state of 0.306 ppm is used to calculate the straight line ($R = 0.998$) which is characterized with the slope of 1.07 ($\sigma = 0.04$) and pK_a of 7.64 ($\sigma = 0.03$) (see panel g in Figure S1 in the supporting information). The Hill plot for ΔG° of FU (**13**) where the total change between the neutral and the deprotonated state (ΔG°_{tot}) of 0.25 kJ/mol is used to calculate the straight line ($R = 0.935$) with the slope of 0.98 ($\sigma = 0.2$) and pK_a of 8.0 ($\sigma = 0.1$) (see panel h in Figure S1 in the supporting information).

Acknowledgment. We thank the Swedish Board for Technical Development and Swedish Natural Science Research (NFR) Council, Swedish Board for Technical Development (NUTEK), Sweden, for generous financial support. We also thank Dr. A. Papchihin and Mr. E. Zamaratski for the preparation of the imidazolo nucleoside. Thanks are due to the Wallenbergstiftelsen, Forskningsrådsnämnden, and University of Uppsala for funds for the purchase of a 500 MHz Bruker AMX NMR spectrometer.

Supporting Information Available: The temperature-dependent (278–358 K at 5 or 10 K intervals) vicinal coupling constants for **1–13** as a function of pD (Tables S1–S7) are available. The Hill plots used for the determination of pK_a of the aglycon in **1–13** from pD-dependent 1H -NMR chemical shifts as well as the determination of pK_a from pD-dependent ΔG° of the $N \rightleftharpoons S$ pseudorotational equilibrium of the sugar moiety are shown in Figure S1 (7 pages). This material is contained in libraries on microfiche, immediately, follows this article in the microfilm version of the journal, and can be ordered from the ACS; see any current masthead page for ordering information.

JO951124A